

RESEARCH

Open Access

Interference management for moving networks in ultra-dense urban scenarios

Yutao Sui^{1*}, Ismail Guvenc² and Tommy Svensson¹

Abstract

The number of users relying on broadband wireless connectivity while riding public transportation vehicles is increasing significantly. One of the promising solutions is to deploy moving base stations on public transportation vehicles to form moving networks (MNs) that serve these vehicular users inside the vehicles. In this study, we investigated the benefits and challenges in deploying MNs in ultra-dense urban scenarios. We identified that the key challenge limiting the performance of MNs in ultra-dense urban scenarios is inter-cell interference, which is exacerbated by the urban canyon effects. To address this challenge, we evaluated different inter-cell interference coordination and multi-antenna interference suppression techniques for MNs. We showed that in using MNs together with effective interference management approaches, the quality of service for users in vehicles can be significantly improved, with negligible impacts on the performance of regular outdoor users.

Keywords: 5G; HetSNet; Interference management; Moving networks; Ultra-dense urban networks; Vehicular users

1 Introduction

The demand for ubiquitous availability of broadband mobile data is exploding. The industry has predicted a 1,000-fold increase in mobile data traffic within the next decade [1-3]. To meet the capacity demand of mobile communication systems, academia and industry are working together closely. The Third Generation Partnership Project (3GPP) has recently standardized the Long Term Evolution-Advanced (LTE-A) networks and has been working on developing its evolution by adding more features to support higher system throughput. Several large scale projects such as EU FP7 Mobile and wireless communications Enablers for the Twenty-twenty Information Society (METIS) and 5GNOW^a [2,4], have also recently started to investigate 5G mobile communication systems, ranging from new radio access interfaces to new system architectures.

With the increasing capabilities of mobile devices and cloud computing, user experiences are not only based on the capacity a mobile communication system can offer but are also determined by the latency of the communication, reliability of the services, and pervasive availability

of the networks. The METIS project describes five features of the next-generation mobile communication systems as '1) amazingly fast, 2) great service in a crowd, 3) ubiquitous things communicating, 4) best experience follows you, and 5) super real-time and reliable connections' [4]. The number of users relying on wireless data connections while riding public transportation vehicles, e.g., buses, trams, and trains, is increasing significantly, because of the high penetration of smart phones, tablets, and increasingly portable notebooks. Users are expecting similar experiences at home, in the office, when stationary or traveling, or commuting. Therefore, in this study, we target a particular user group, i.e., vehicular users located in well-isolated public transportation vehicles.

Serving these vehicular users efficiently has been a problem that has recently attracted significant attention [5-8]. In a coverage-limited scenario, e.g., high-speed trains or inter-city coaches in suburban areas, the vehicular penetration loss (VPL)^b is identified as one of the biggest factors that limits the performance for vehicular users [5]. According to the measurements in [9], VPL can be as high as 25 dB in a minivan at the frequency of 2.4-GHz, and higher VPLs are foreseeable in well-isolated vehicles and at higher frequency bands, e.g., the 3.6-GHz band allocated to future mobile communication

*Correspondence: sui.yutao@chalmers.se

¹Department of Signals and Systems, Chalmers University of Technology, EDIT-huset, Hörsalsvägen 9-11 Gothenburg, SE-41296, Sweden
Full list of author information is available at the end of the article

systems [10]. One of the most promising solutions to better serve vehicular users is to use moving relay nodes (MRNs) mounted on top of public transportation vehicles [6,7,11]. An important advantage of using MRNs is that by the proper placement of the antennas on a vehicle, the VPL can be circumvented, and thereby, the quality of service (QoS) for the users can be significantly improved. Moreover, compared with regular user equipment (UE) devices, an MRN has fewer constraints in terms of transmit power and transceiver complexity, and therefore, more antennas and advanced signal processing algorithms can be used in MRNs to further boost performance.

To the best of our knowledge, all existing studies related to MRNs either deal with system architecture issues or study the performance of MRNs in simplified scenarios (see Section 2). There has been no thorough investigation on using MRNs in typical outdoor urban scenarios. In typical outdoor urban deployments, because of the densely deployed small cells and street canyon effects, complicated inter-cell interference becomes one of the key factors limiting the performance of mobile communication systems. To better understand the practical challenges of using MRNs in ultra-dense urban scenarios, in this study, we extend our earlier investigations on MRNs in [7,11,12] in several aspects. In this study, we extend the studies of half-duplex MRNs to full-duplex moving networks (MNs). Both MRNs and MNs form their own cells inside public transportation vehicles to serve the vehicular UE (VUE) devices on board, and communicate with the macro BSs through the radio interface. However, the MRNs can only work in a half-duplex fashion, as the backhaul links and access links of MRNs are assumed to operate in the same frequency band. In the vision of METIS, more bandwidth can be freed up for small cell deployment in the 5G system. Therefore, it becomes feasible in the 5G systems to have vehicles constitutes a full-duplex MN with backhaul and access links on different frequency bands.

We focus on the deployment of MNs on public transportation vehicles in an ultra-dense urban area with a practical densely deployed heterogeneous and small cell networks (HetSNets) framework defined by the test case ‘dense urban information society’ in the EU 5G project METIS [4]^c. More specifically, an MN communicates with a macro BS via its backhaul link and forms a small cell inside a public transportation vehicle. Instead of being served directly by the macro BS, the VUEs located inside a public transportation vehicle are offloaded to the vehicle’s MN. In such a setup, the complicated interference situation becomes a significant problem, where MNs are subject to inter-cell interference from both macro and micro cells. As an example, when MNs are passing through the small cells, the access links of MNs experience dynamic fluctuations of interference power. Moreover, MNs may

also potentially bring unexpected interference challenges into the system.

Contributions: In this study, we first identify the challenges in deploying MNs in ultra-dense urban HetSNets scenarios in terms of interference situations. To exploit the benefits of MNs, based on the availability of channel state information (CSI) and multi-antenna deployments, we then apply and compare various inter-cell interference coordination (ICIC) and interference cancellation schemes to alleviate the impact of inter-cell interference on MNs. Furthermore, the fairness between VUEs and regular outdoor UEs is also evaluated. We show that compared with serving the VUEs directly from macro BSs, by using MNs, the QoS at VUEs can be significantly improved without sacrificing the performance of regular outdoor UEs. Therefore, MNs can bring noticeable benefits to future mobile communication systems.

The paper is organized as follows. In Section 2, we introduce previous studies related to MNs and various ICIC solutions used in HetSNets. Section 3 presents the detailed system model that we used to evaluate the performance of MNs. In Sections 4 and 5, we discuss both the time domain and multi-antenna solutions considered in this study to cope with inter-cell interference challenges for backhaul links of MNs and macro UEs. The ICIC scheme used for micro cells is discussed in Section 6, and the detailed evaluation results using the METIS 5G simulation framework are presented in Section 7. In Section 8, we discuss the complexity of the schemes considered in this paper, the constraints in the current LTE-A systems that limit further performance improvement of MNs and some important future research directions using MNs. Section 9 concludes the paper.

2 Related studies

Because the demand for mobile data capacity is growing, especially in urban areas, network densification is inevitable. HetSNets are identified as one of the key solutions to address the capacity demand of next-generation mobile communication systems, as they maximize the reuse of existing spectra by deploying more nodes in a given area [1,3,13]. In HetSNets, various low-power nodes, i.e., remote radio heads (RRHs), micro and femto BSs, and fixed-relay nodes (FRNs), are deployed underlying traditional high power macro BSs. In this way, the low-power nodes can meet the capacity needs in certain hot spot areas while high-power macro BSs are used to provide basic coverage. In the study of the 5G mobile communication system, a HetSNets deployment has been considered from the very beginning [3,4]. For example, in the test case ‘dense urban information society’ of the METIS project, a dedicated HetSNets deployment called the *Madrid grid model* was developed based on the characteristics of typical European cities [14].

In [15], it is shown that in an ideal HetSNets setup, even though interference becomes severe as transmitters get closer, network densification can still bring significant gains to a wireless communication system. In practical deployment of HetSNets, to improve the small cell coverage and achieve more offloading gain, cell range expansion (CRE) is introduced in 3GPP LTE Rel-10 ([16,17] Ch. 24 and 31). In CRE, a positive bias is added to the reference signal received power (RSRP) of small cells, and thereby more UEs can be offloaded to small cells. Using CRE, the coverage of small cells can be expanded to offload more macro users to small cells, and the overall uplink performance of the network can be improved [1,17,18]. However, because of severe inter-cell interference, CRE causes downlink performance degradation, especially for the cell-edge UEs of the small cells.

Therefore, to realize the CRE gain and protect victim UEs, it is critical to use ICIC schemes in the deployment of HetSNets [1,13,19]. Both time and frequency domain solutions have been extensively studied to cope with the inter-cell interference [20,21]. The use of almost blank subframes (ABSs) is standardized in 3GPP LTE Rel-10 as a part of the enhanced inter-cell interference coordination (eICIC) framework to protect UEs that are subject to excessive co-channel interference ([16] Ch. 31.2.2) [18,22-24]. Moreover, the use of multi-antennas to suppress interference is also studied for practical deployments ([20] Ch. 5). For example, network-assisted interference cancellation has been studied for 3GPP LTE Rel-12 [25]. In later sections, we discuss the ICIC schemes, used in this study, in further detail.

Providing ubiquitous service experience for users on well-isolated high-speed vehicles is very challenging because of the speed of the vehicles and the severe attenuation of the received signal caused by the VPL. Several solutions using elements of existing systems, such as deploying dedicated macro BSs, or using layer-1 repeaters and WiFi access points, have been discussed in 3GPP [5]. These solutions, however, are temporary and mainly aim at offering a basic coverage for VUEs rather than capacity improvement.

To better serve the VUEs, using MRNs has been proposed and studied in [5-7,12,26-29]. The idea of using mobile devices to relay information to UEs outside the coverage of a BS is not new. Mobile devices can form a mobile *ad hoc* network (MANET) to enable communications between mobile devices directly without (or with limited support of) network infrastructure [30]. Nowadays, MANET attracts more attention because of the investigation into device-to-device (D2D) communications in the next-generation mobile communication systems [31-33]. The mobile communication system can benefit from mobile-device-enabled relaying in several

different ways. For example, with the approach in [34], using a nomadic network formed by randomly parked vehicles to relay data from BSs to UEs, significant energy savings can be achieved. Other relevant studies show that in using D2D-enabled relaying in mobile communication systems, the coverage of a cellular network can be extended, the network capacity can be improved, and the outage probability of the communication can be reduced [32,33,35-37]. Interference management in MANET is very challenging. In a MANET without central control nodes, interference management based on power control or coordination between different nodes can only be implemented in a distributed manner [38], which usually leads to local or suboptimal solutions. If a central control node is available, more effective interference and resource management algorithms can be implemented, and therefore, MANET can bring more gains to the current mobile communication systems. For example, studies in [36,39,40] show that with effective interference management and resource allocation methods, a mobile communication system can benefit in various ways by using D2D-enabled communication underlying the coverage of a BS. However, MANET provides limited support to high-mobility users. Because the topology of a MANET may change very fast, it may not always be possible to find available nodes to relay the information. As pointed out in Section 3, complicated inter-cell interference is one of the biggest factors limiting the performance gains that can be obtained using MNs. Therefore, in an interference-limited scenario with high-mobility users, e.g., to serve VUEs in a densely deployed urban scenario, the MANET solutions cannot be directly applied.

Previous studies show that by using MRNs, in a coverage-limited scenario [6,7,11] or scenarios with insignificant interference [12,27,28], both the QoS of VUEs and the system throughput can be significantly improved. From a system perspective, several architectures have been proposed and compared for deploying MRNs to current mobile systems in [5,8]. Moreover, it has been identified that the backhaul links are the bottlenecks to further improve the performance of MRNs [11,28]. Compared with regular UEs, MRNs have fewer constraints in terms of transmit power and transceiver complexity, and thereby, more antennas and advanced signal processing algorithms can be used in MRNs to further boost performance. In [41,42], it is shown that by using the so-called predictor antennas mounted on top of a vehicle, reliable CSI for the backhaul links of MRNs can be obtained to support various multi-antenna operations. Therefore, the throughput of the backhaul links of MRNs can be significantly improved. In [29], the energy efficiency aspects of using MRNs are studied, showing that the energy consumption of the network can be reduced by using MRNs, when compared with serving the VUEs

directly from the macro BSs. The mobility management aspects of MRNs have been studied in [8,12,43]. In [12], a generalized framework to optimize the parameters related to the handovers with MRNs was proposed. In [43], it is shown that by using MRNs on high-speed trains, the number of ping-pong handovers and handover failures can be significantly reduced.

In the EU 5G project METIS, based on the study of MRNs, the concept of MNs has been developed and integrated as part of the METIS 5G system concept [44]. In METIS, the concept of MNs not only covers mobility-robust high data-rate communication links for VUEs but also includes flexible demand-driven network deployment. The MNs are also envisioned to provide low-latency services for road safety and traffic efficiency [44]. To understand the impact of deploying MNs to an ultra-dense urban HetSNets scenario, in this study, we evaluated the performance of MNs within the HetSNets framework defined by METIS. In the next section, we describe the detailed METIS setup to provide a background for the performance investigation of MNs.

3 System model for moving networks

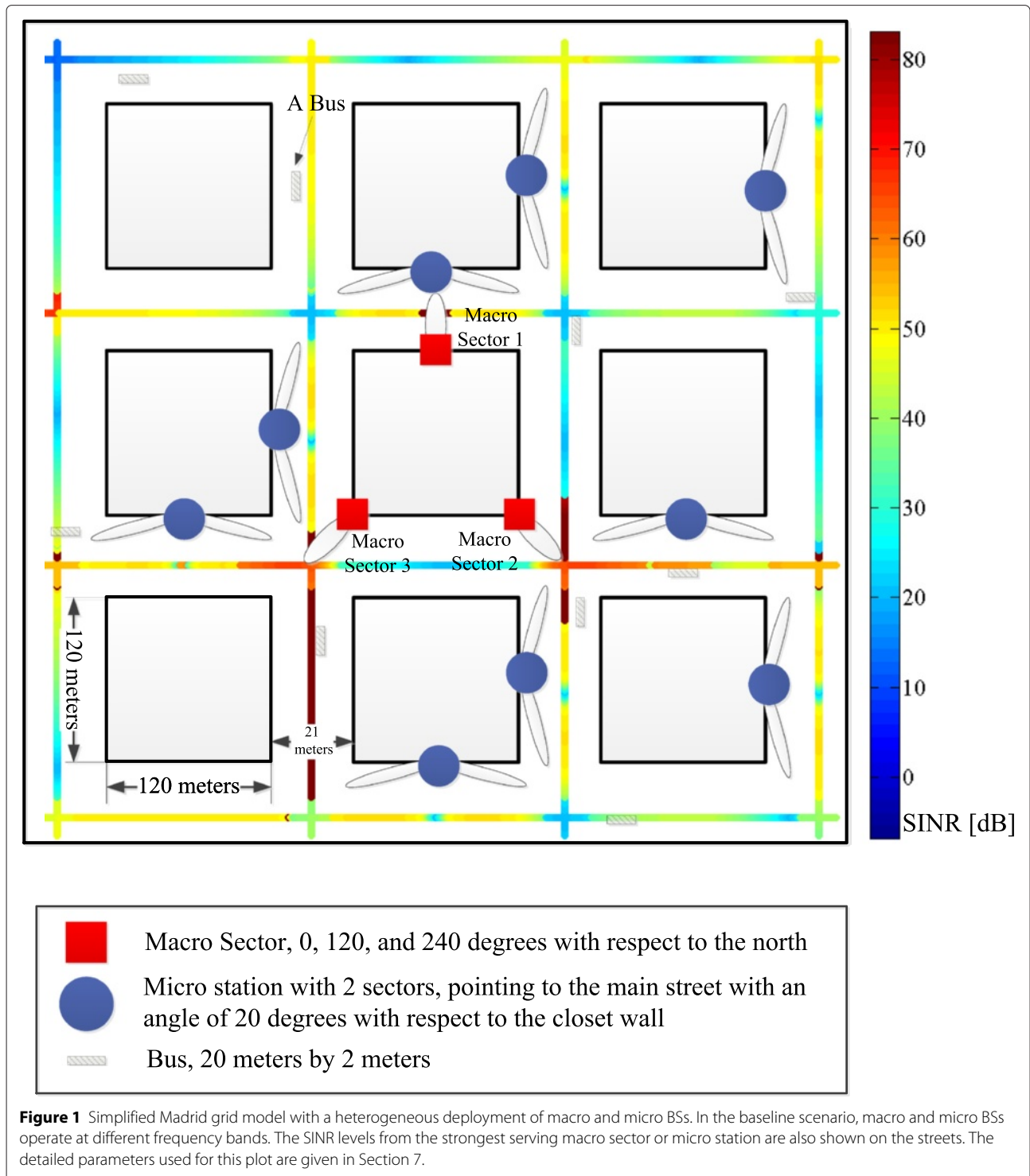
We considered the downlink of a densely deployed mobile network in a typical urban setup, which was developed and used in the METIS project [14]. To facilitate the comparison of different schemes, based on the Madrid grid model, an abstract and simplified deployment model is suggested by METIS, as shown in Figure 1, where heterogeneously deployed macro and micro BSs are considered. In this study, we consider the calibration deployment given in Table 3.7 in [14], where macro BSs offer basic coverage, and micro BSs are used for capacity-demanding applications and local coverage. A macro BS has three sectors and transmits at the 800-MHz band with a 20-MHz bandwidth. Each micro BS has two sectors and transmits at the 2.6-GHz band with an 80-MHz bandwidth. We assume the general scenario that an MN is deployed on a public transportation vehicle, e.g., a bus or a tram. Following the 3GPP convention, we name the link between an MN and a macro BS as the backhaul link and the link between an MN and its VUEs as the access link, respectively. The backhaul of the MN communicates with a macro BS sector at 800-MHz, and the access link operates at 2.6-GHz to serve the users inside the vehicle. Public transportation vehicles enter each street through a Poisson process with an inter-arrival time of 2 min and a fixed velocity of 50 km/h ([14] Sec. 9.2). Since the backhaul links and access links operate at different frequency bands, in this study, we assume that MNs work in a full-duplex mode.

The inter-cell interference experienced by the backhaul links of MNs is very similar to the inter-cell interference

faced by the VUEs, if the backhaul links are served directly by macro cells. Therefore, some of the traditional ICIC schemes, e.g., using ABS (see Section 4), can be directly applied. Introducing MNs to a mobile communication system brings in more opportunities to better serve the VUEs but also creates more challenges. Preliminary studies in METIS show that without using any ICIC schemes or interference cancellation, there are limited gains in using MNs to serve VUEs in densely deployed urban scenarios ([45] pp. 33), because the MNs are operating mostly at the same interference-limited scenario as regular outdoor UEs. This is discussed in more detail in Section 3.1. Therefore, techniques for alleviating the impact of inter-cell interference become important when using MNs in a densely deployed urban scenario. Unlike the regular UEs, MNs are less constrained by size, power, and transceiver complexities, and therefore more antenna elements can be deployed and more advanced signal processing schemes can be implemented at the MNs to combat the interference. In Section 5, we present multi-antenna techniques for the backhaul receivers of MNs to combat inter-cell interference.

Furthermore, if we simply treat an MN as a regular UE with high data-rate demand and do not consider the QoS of each of the individual VUEs served by the MN, the scheduler at the BSs may not allocate enough resources to the MN. This is because the scheduler at the BSs needs to ensure fairness between different UEs sharing the same time and frequency resources. Therefore, an unfair situation may be faced by the VUEs. Hence, in this study, we regard an MN as a super user that aggregates the traffic from all the VUEs it serves. Thus, when we design the scheduling algorithm, the number of VUEs served by an MN has to be taken into account. We analyze this problem further in Section 3.2.

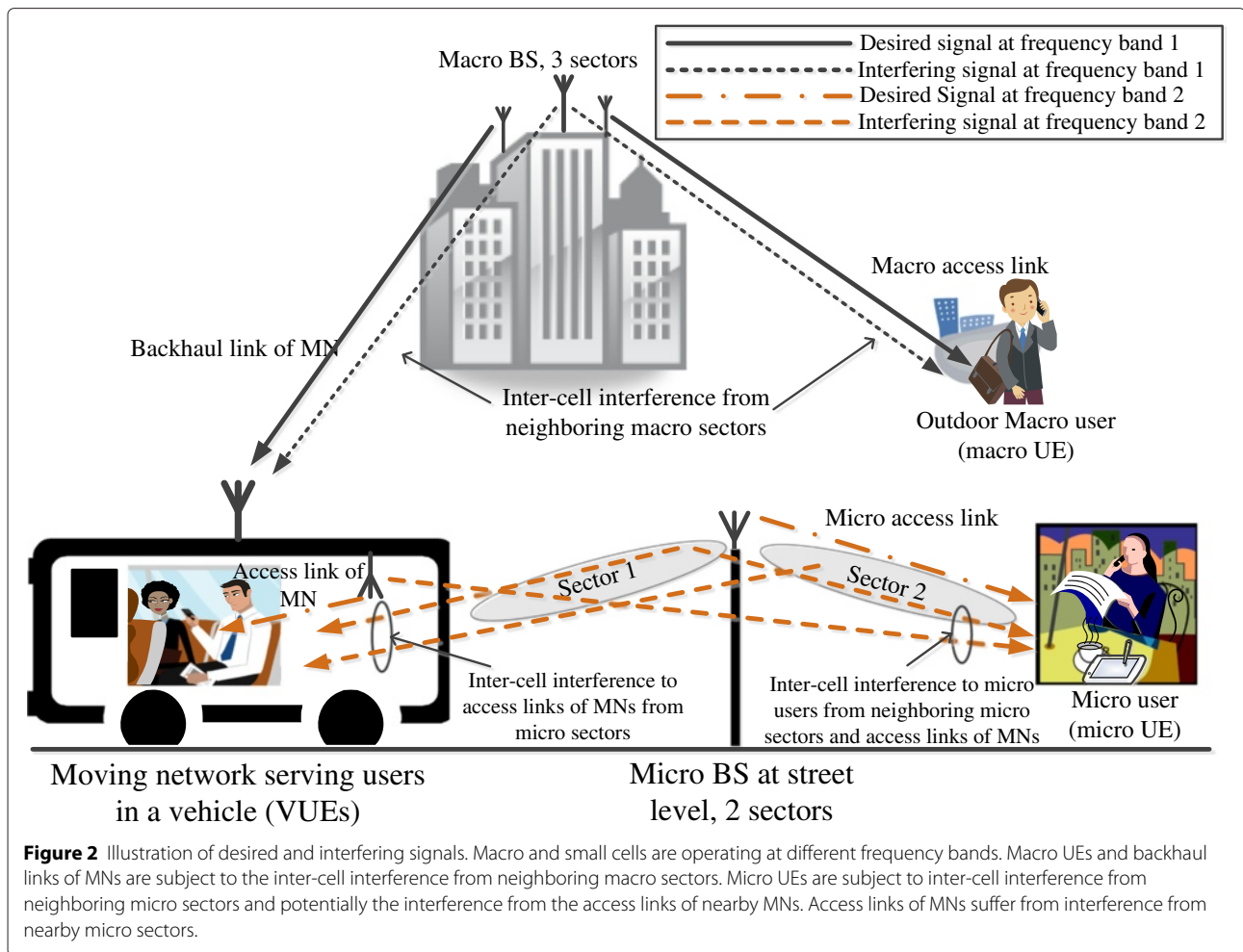
In this study, we consider an orthogonal frequency-division multiple access (OFDMA)-based system which is the multiple access technology for the existing LTE-A systems. Corresponding parameters such as the sub-carrier spacing, the physical resource block (PRB) size, the sub-frame length, the modulation and coding schemes, and the link adaptation constraints that are defined in the frequency division duplex (FDD) LTE-A specifications are adopted throughout the paper. As the current FDD LTE-A system supports a maximum of 20 MHz bandwidth for a specific carrier frequency, we consider an intra-carrier aggregation configuration for the 80-MHz bandwidth used by the micro cells. A PRB, which consists of 12 subcarriers, with a duration of 0.5 ms, is the basic unit of resource allocation for a user in an LTE-A system. In most of the cases, the channel coherence bandwidth and time are much larger than the size of a PRB. Thus, we can assume a frequency flat-fading channel within a PRB.



3.1 Interference identification for MNs

As demonstrated in [7,11], in a noise-limited system, MNs can improve the QoS of vehicular UEs, because the backhaul links of MNs have better propagation conditions and an MN can circumvent the VPL. In an ultra-dense urban scenario, however, situations are very different for both

the backhaul and access links of MNs, particularly because of different central frequency propagation environments and bandwidths. Figure 2 illustrates the interference situations for different users. There is no interference between macro and micro cells, as they operate on different frequency bands. Macro users and the backhaul links of MNs



experience interference from neighboring macro sectors. Micro users are subject to interference from micro sectors close by and the access links of MNs. A vehicular user can experience interference from micro cells and potentially by the access links of other close-by MNs.

Figure 1 plots the signal-to-interference-plus-noise ratio (SINR) that an outdoor user experiences in the considered Madrid grid set up, assuming the user always associates with the strongest cell (5 dB CRE is considered for the micro cells, and detailed parameters used for the plot are given in Section 7). As we can see from the SINR plot, in an ultra-dense urban scenario, because of inter-cell interference, the SINR can still be low, even when a user is close to a BS, e.g., between Macro sectors 2 and 3. The same situation applies for the MNs. Although, MNs can circumvent VPL and improve the signal-to-noise ratio (SNR) at the VUEs, in a densely deployed scenario, the severe inter-cell interference has a noticeable impact on the received SINR. To illustrate this, for the deployment scenario shown in Figure 1, Figure 3 shows an example of the SNR and SINR cumulative distribution function

(cdf) at the backhaul links of MNs and the VUEs when the VPL is 15 dB. Compared with when VUEs are directly served by macro cells, the SNR is much improved via MNs because of better propagation conditions and the circumvention of VPL. However, SINR is only slightly improved by using MNs. Although the desired signal strength can be improved at the backhaul antennas, the desired signal subject to significant inter-cell interference. Furthermore, different from the traditional hexagonal cell deployment model, in a Madrid grid model, interference situations experienced by the receivers are more complicated because of urban canyon effects and may degrade the SINR observed at an MN.

The access links of MNs are assumed to transmit at the same frequency bands as the micro BSs. Although micro BSs transmit at a much lower power than the macro BSs, the interference they bring to the access links of MNs is still significant. This is because micro BSs are densely deployed at street level (around 80 m apart from each other in the Madrid grid baseline case), and, in the worst case scenario, the access link of an MN can be subject

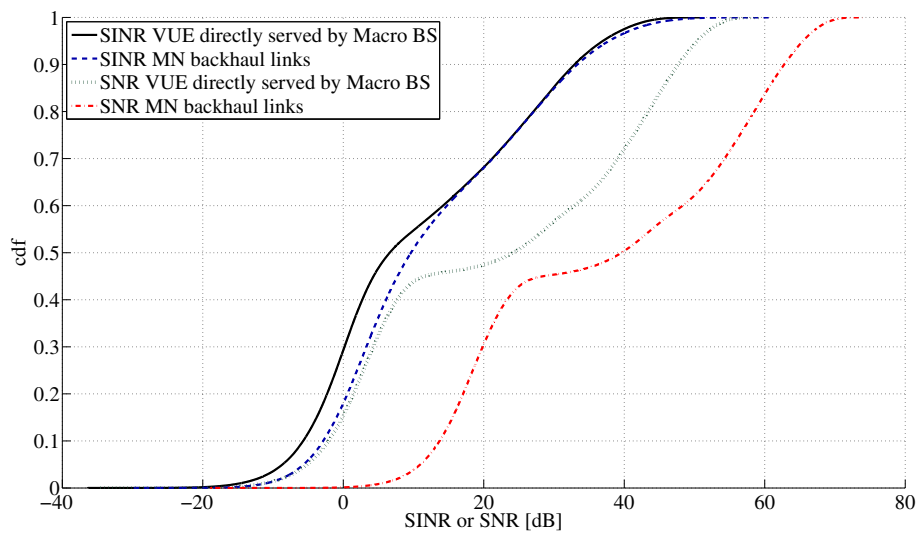


Figure 3 SNR and SINR plot of VUEs at 15 dB VPL. The detailed parameters used for this plot are given in Section 7. The solid black line is the SINR at VUEs when the VUEs are served directly by the macro BS. The dashed blue line is the SINR of the backhaul links of MNs. The dotted dark green line is the SNR at VUEs when the VUEs are served directly by the macro BS. The dash-dot red line is the SNR of the backhaul links of MNs.

to interference from several micro BS sectors at the same time. As shown in Figure 4, without interference coordination methods, even though the available bandwidth of the access links of MNs is large, the access links of MNs may not always accommodate the traffic from their backhaul links.

Therefore, to improve the performance of VUEs served via MNs, we have to alleviate the impact of inter-cell interference, both for the backhaul and access links of MNs. The methods used to improve the performance of backhaul links are discussed in Sections 4 and 5, while the

ICIC scheme used to protect access links is outlined in Section 6.

The access links of the MNs might also cause interference with each other. However, in the scenario that we consider in this study, the interference between the access links of the MNs has negligible impact on the throughput of the VUEs. There are two main reasons for this. First, the access links of MNs only need to accommodate the traffic from their backhaul links. Because of the relatively large bandwidth compared with the backhaul links, and short distance (around 5 to 10 m) between the access

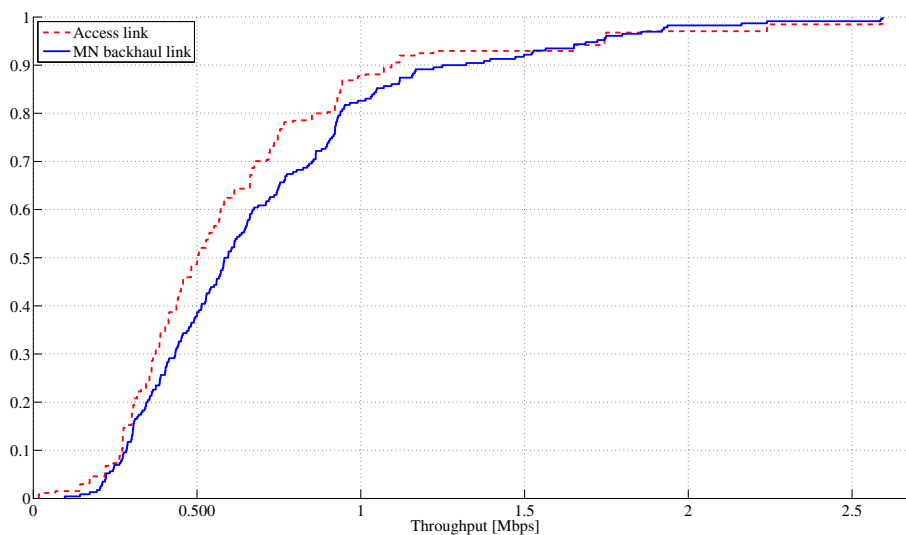


Figure 4 An example for the throughput cdf of an MN without ICIC in micro cells. The schemes used for MN backhaul is MRC combining with four antennas, and the VPL is at 15 dB. The detailed parameters used for this plot are given in Section 7. The dashed red line is the throughput of the access links. The solid blue line is the throughput of the backhaul links of MNs.

link antennas and the VUEs, a high-transmit power is not needed for the access links of MNs. Second, the interference generated by the access link of an MN is attenuated twice by the VPL, from its own vehicle and from the other vehicles. We observed similar effects in our previous studies in [12,28], which showed that the vehicle itself can help to reduce the impact of co-channel interference. This is very beneficial from a system perspective, because the frequency can be reused more efficiently. Therefore, in this study, we do not consider any interference management scheme between the access links of the MNs.

3.2 Fairness between regular UEs and VUEs

Besides the study of different ICIC schemes that can be used for MNs, our study also aims at improving the performance of VUEs without sacrificing the fairness between VUEs and regular outdoor UEs. We use proportional fairness (PF)-based resource allocation to ensure a balance between system throughput and fairness among all the users [46]. We assume a full buffer traffic situation as well as the same priorities for all the UEs, i.e., VUEs, macro UEs, and micro UEs. Furthermore, in this study, each MN is regarded as a super user that aggregates the data traffic of all its VUEs. In this section, we briefly describe how to modify the PF scheduler to integrate the MNs and their VUEs into the scheduling decisions.

In a network without MNs, the throughput of N_u users is proportionally fair [46], if it maximizes the following objective function:

$$f_1 = \sum_{u=1}^{N_u} \log(s(u)), \quad (1)$$

where $s(u)$, ($u = 1, 2, \dots, N_u$), is the average throughput of the u th user. Note that in an OFDMA system, the minimum scheduling granularity is given by a PRB. Without loss of generality, we use $b(l, m, u)$ to denote the scheduling decision for the u th user in m th PRB in the l th subframe, i.e.,

$$b(l, m, u) = \begin{cases} 1, & \text{if user } u \text{ is assigned at } (l, m) \\ 0, & \text{if user } u \text{ is not assigned at } (l, m) \end{cases}. \quad (2)$$

In a general case, $b(l, m, u)$ is determined by a PF scheduler as follows [47,48]. First, for each user u , its throughput at m th PRB in the l th subframe is calculated as $r(l, m, u)$. Based on the SINR information, there are several ways to calculate the throughput $r(l, m, u)$, e.g., look-up tables or variations of the Shannon capacity equation [49,50]. In this study, we use the SINR look-up table method [50]. Then, a user u^* is selected at (l, m) as:

$$u^*(l, m) = \arg \max_{u \in \{1, 2, \dots, N_u\}} \left(\frac{r(l, m, u)}{\mu(l, u)} \right), \quad (3)$$

where $\mu(l, u)$ is the average throughput of user u , which is updated in each subframe as:

$$\mu(l+1, u) = (1 - \varepsilon) \mu(l, u) + \frac{\varepsilon}{M} \sum_{m=1}^M r(l, m, u) b(l, m, u). \quad (4)$$

In Equation 4, M is the total number of PRBs in each subframe, and $0 \leq \varepsilon \leq 1$ is an averaging constant, which is usually set to 0.5 [47]. Finally, the resource assignment is determined as:

$$b(l, m, u) = \begin{cases} 1, & \text{if } u = u^*(l, m) \\ 0, & \text{otherwise} \end{cases}. \quad (5)$$

When the MNs are introduced into the system, to ensure fairness between VUEs and macro UEs, the PF scheduler needs to be modified in order to take the aggregate traffic carried by the MNs into account. As mentioned before, we treat an MN as a super user that aggregates the traffic of all the VUEs it serves. The MNs whose backhaul links are served by macro cells share the same resources as macro UEs. Since several VUEs are served by one MN, the throughput of the MN backhaul link needs to be scaled by the number of VUEs that it serves. Otherwise, the backhaul link of an MN will not get a fair scheduling assignment. Let there be a total of N_m MNs in the system, and let i_v denote the number of active VUEs on the v th MN, where $v = 1, 2, \dots, N_m$. Then, as opposed to using Equation 1, the objective function of the PF scheduler is modified as:

$$f_2 = \sum_{u=1}^{N_u} \log(s(u)) + \sum_{v=1}^{N_m} \log\left(\frac{s(v)}{i_v}\right), \quad (6)$$

where $s(v)$, ($v = 1, 2, \dots, N_m$) is the average throughput of the backhaul link of the v th MN. In this study, the number of active VUEs served by an MN is a uniformly distributed discrete random variable, with $i_v \sim \mathcal{U}(1, 50)$, where \mathcal{U} denotes uniform distribution. The difference between Equation 1 and Equation 6 is that the traffic of the backhaul link of each MN is averaged by the number of its VUEs. The scheduling algorithm involving MNs and the time domain ICIC scheme is described in Section 4.2.

As mentioned before, in an interference-limited scenario, certain users at the cell edges are subject to strong interference from neighboring cells. Although PF scheduling is a way to achieve a balance between user fairness and system throughput, it cannot alleviate the impact of interference. In the following sections, we discuss the use of both time domain methods and multi-antenna solutions to alleviate the impact of interference, and the PF scheduling is used together with these schemes to ensure fair resource allocation among all the UEs.

4 Time domain interference coordination for the backhaul links of MNs

As mentioned in Section 2, using ABSs is standardized in 3GPP to protect victim UEs that are subject to excessive co-channel interference. The ABSs can be configured by either macro or micro cells, and different ABSs patterns and density can be configured by each individual cell to offer various levels of protection to UEs influenced by co-channel interference ([16] Ch. 31)[22-24]. The benefits of using ABSs are that it is standard compliant and can be combined with other existing ICIC methods, e.g., frequency reuse, power control, or various multi-antenna solutions.

As mentioned in Section 3, we consider a macro BS that has three sectors. Three types of macro UEs are identified in the system. The first group of UEs has high SINR values, which means these UEs are in the cell center, and are less affected by inter-cell interference. We label this group of UEs as type 1. The second group of UEs experience higher interference from one of the macro BS sectors, i.e., the interference power from one sector is much larger than the other interfering sector. We label this group of UEs as type 2. The third group of UEs experience similar interference power from both interfering sectors. We label this group of UEs as type 3. Obviously, type 2 and 3 UEs need to be protected from interference.

Figure 5 shows an example of the ABS configurations of the three sectors of a macro BS. Scheduling restrictions can be applied to achieve different levels of protection for the UEs. The idea of the scheduling restriction is to restrict the UEs that are in good channel conditions to the non-protected sub-frames, so that more resources can be made available for the victim UEs. To be more specific, the protected resources are reserved for victim UEs that are subject to strong inter-cell interference. However, these victim UEs can also be scheduled in the non-protected sub-frames, if there are available resources and/or the throughput of one of the protected resources is too low to maintain good fairness between the UEs. Therefore, type 1 UEs are not subject to interference, so they are strictly

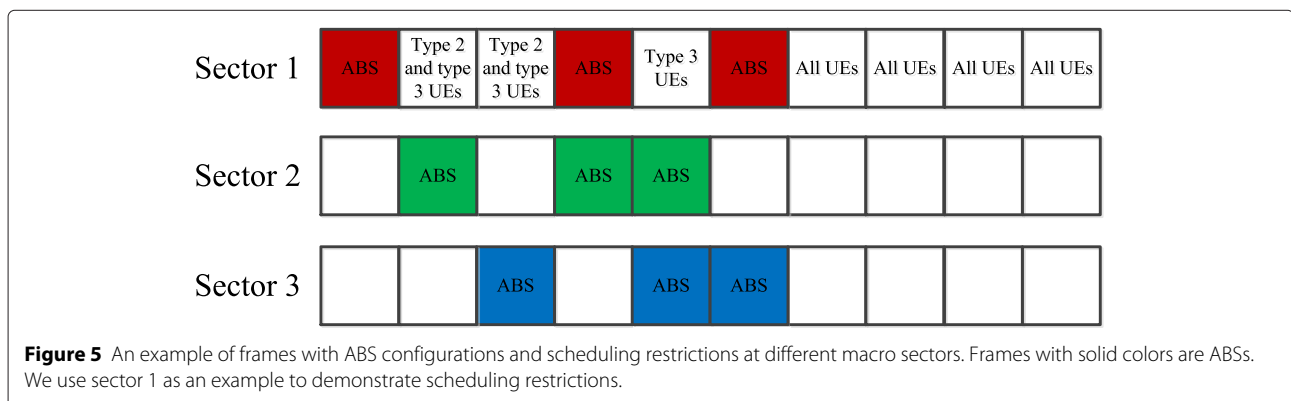
scheduled in the unprotected sub-frames. Type 2 UEs are restricted to sub-frames where their dominant interferer is muted (recall that one significant interferer is observed by a type 2 UE) and where the sub-frames are unprotected. No scheduling restrictions are applied to type 3 UEs.

Therefore, two questions need to be answered to use the time domain ICIC method: 1) how to configure the number of ABSs for each macro BS sector, and 2) how to classify the UEs and schedule them to achieve a balance between maximum protection for the victim UEs and the system throughput. Previous studies show that even in simplified setups, a joint optimization of these two problems is very difficult [23,47,51]. Next, we briefly review and discuss the possible ways to address these two problems.

4.1 Configuration of ABSs

The ABSs patterns of each cell may be dynamically changed. For example, in LTE-A systems, the duty cycle of ABSs can be as short as 40 ms [22] ([16] Ch. 31). However, for practical reasons, e.g., for obtaining traffic distribution statistics and considering the reconfiguration overhead,^d the time scales of changing ABSs patterns could be at least in the order of a few minutes [22,23].

When considering different scheduling algorithms, QoS constraints, and other factors, it is challenging to obtain an optimal ABS pattern across multiple cells within a reasonable time. The ABS pattern optimization problem is shown to be NP-hard in a multi-cell full buffer traffic scenario [23]. Previous studies either consider fixed ABS patterns based on traffic distribution statics or use sub-optimal solutions based on simplified assumptions [47,51]. In this study, we consider the use of fixed ABSs patterns (described in the appendix). We consider two setups, i.e., 12 ABSs out of 40 frames (30%) and 15 ABSs out of 40 frames (37.5%). In the next section, we discuss how to classify the UEs and the criteria of identifying their strong interferers, as well as how to incorporate the PF scheduling with the scheduling restrictions.



4.2 Scheduling restriction schemes

After determining the ABS patterns of each cell, the next step is to determine how to schedule the three types of UEs. Several criteria have been proposed in determining scheduling restrictions. In [52,53], cell edge UEs and cell center UEs are scheduled in protected and non-protected resources, respectively. In [47], scheduling restrictions are applied based on the channel quality differences between protected and non-protected resources. In our study, we apply the generalized method in [47] to classify the three types of UEs. The framework proposed in [47] takes several factors into account, e.g., user distribution and the ratio between protected and non-protected resources, to decide how to apply the scheduling restrictions. While in [47] only two cells are considered, the method can easily be extended to our scenario by applying pairwise comparisons. Next, we briefly introduce the method used in [47] and discuss how to use it to determine the three different types of UEs in this study.

We begin with a two-cell setup, and we use macro BS sector 1 as an example. The user sets for macro UEs and MNs are $\mathcal{M} \triangleq \{1, 2, \dots, N_u\}$ and $\mathcal{V} \triangleq \{1, 2, \dots, N_m\}$, respectively. In total, $N = N_u + N_m$ devices connect to macro BS sector 1, and the interference is from macro BS sector 2. The macro BS sector 2 configures ABSs patterns, and macro BS sector 1 makes the scheduling decisions accordingly. From the perspective of BS sector 1, we define two sets of PRBs, i.e., protected PRBs \mathcal{R}_p and non-protected PRBs \mathcal{R}_{np} . Denote the total number of protected PRBs as $B_p = |\mathcal{R}_p|$, and the total number of non-protected PRBs as $B_{np} = |\mathcal{R}_{np}|$, where $|\cdot|$ is the cardinality of a set. With scheduling restrictions, users served by BS sector 1 can be partitioned into three sets: $\mathcal{S}_1 = \{\text{users only scheduled in } \mathcal{R}_p\}$, $\mathcal{S}_2 = \{\text{users only scheduled in } \mathcal{R}_{np}\}$, and $\mathcal{S}_3 = \{\text{users can be scheduled both in } \mathcal{R}_p \text{ and } \mathcal{R}_{np}\}$.

As mentioned in Section 3.2, the throughput of the backhaul links of MNs needs to be scaled by the number of VUEs that it serves. Therefore, for device n , its throughput at m th PRB in the l th subframe is calculated as:

$$r(l, m, n) = \begin{cases} r(l, m, u), & n \in \mathcal{M} \\ \frac{r(l, m, v)}{i_v}, & n \in \mathcal{V} \end{cases}, \quad (7)$$

where $r(l, m, u)$, ($u = 1, 2, \dots, N_u$) and $r(l, m, v)$, ($v = 1, 2, \dots, N_m$) are the throughput of the u th macro UE and the backhaul link of the v th MN at m th PRB in the l th subframe, respectively. The number of VUEs served by the v th MN is i_v . The PF scheduler at BS sector 1 is restricted to the subset of users, i.e., $(\mathcal{S}_1 \cup \mathcal{S}_3)$ and $(\mathcal{S}_2 \cup \mathcal{S}_3)$. The PF scheduling algorithm can be applied with the following modification to the user selection method:

$$n^*(l, m) = \begin{cases} \arg \max_{n \in (\mathcal{S}_1 \cup \mathcal{S}_3)} \left(\frac{r(l, m, n)}{\mu(l, n)} \right), & \text{if } (l, m) \in \mathcal{R}_p \\ \arg \max_{n \in (\mathcal{S}_2 \cup \mathcal{S}_3)} \left(\frac{r(l, m, n)}{\mu(l, n)} \right) & \text{if } (l, m) \in \mathcal{R}_{np} \end{cases}, \quad (8)$$

where $\mu(l, m)$ is updated as given in Equation 4 with the instantaneous rate calculated by Equation 7.

In order to apply the scheduling restrictions for the PF scheduling, we have to properly partitioned the users. It is shown in [47] that at most one user can be in set \mathcal{S}_3 . Let $s(n)$ denote the average throughput of device n , with scheduling restriction, our objective function of a PF scheduler becomes:

$$g = \sum_{n=1}^N \log(s(n)) \\ = \sum_{n=1}^N \log \left(\frac{1}{LM} (r_p(n) b_p(n) + r_{np}(n) b_{np}(n)) \right) \quad (9)$$

where L is the total number of subframes in which $r_p(n)$ and $r_{np}(n)$ are observed. In this study, we set L as the number of subframes in one ABS duty cycle. Moreover, $r_p(n)$ and $r_{np}(n)$ are average rate of the device n over \mathcal{R}_p and \mathcal{R}_{np} , respectively. In addition,

$$b_p(n) = \sum_{(l, m) \in \mathcal{R}_p} b(l, m, n), \quad (10)$$

$$b_{np}(n) = \sum_{(l, m) \in \mathcal{R}_{np}} b(l, m, n). \quad (11)$$

The detailed solution of how to maximize the proportional fairness metric in Equation 9 in a two cell setup is given in [47]. Next, we shortly revisit the solution to facilitate our discussion. The main idea of the solution is first to identify the users with large quality difference between protected and non-protected resources, and then schedule the users accordingly.

In [47], in order to solve the problem, a function $d(n)$ is defined as:

$$d(n) = \begin{cases} \infty, & \text{if } n = 0 \\ \frac{B_p}{B_{np}} \frac{r_p(n)}{r_{np}(n)} & \text{if } n = 1, 2, \dots, N \end{cases}. \quad (12)$$

Recall that B_p and B_{np} are the total number of protected and non-protected PRBs, and $r_p(n)$ and $r_{np}(n)$ are the average rates of device n over the protected and non-protected PRBs, respectively. Therefore, $d(n)$ measures channel quality difference for the n th device over the protected and non-protected PRBs. When $d(n)$ is large, it indicates that the n th device is sensitive to the interference in the unprotected resources and thus it benefits largely from being scheduled to the protected resources. One assumption made in Equation 12 is that by appropriate network planning and UE association, there is no user n such that $r_p(n) = r_{np}(n) = 0$, i.e., no user has

zero throughput. Furthermore, a dummy user $n = 0$ with $d(0) = \infty$ is defined for mathematical correctness of the problem formulation. The solution that maximizes Equation 9 is given in [47], and we summarize the solution in the following paragraph. The step by step derivations are given in the appendix of [47].

The N devices, including both macro UEs and MNs, are sorted descendingly according to Equation 12, i.e., $d(n-1) \geq d(n)$, for $n = 1, 2, \dots, N$, and:

$$\begin{cases} b_p(n) = \frac{B_p}{\lambda_p}, b_{np}(n) = 0, & \text{if } n = 1, \dots, K \\ b_p(n) = B_p \frac{\alpha}{\lambda_p}, b_{np}(n) = B_{np} \frac{1-\alpha}{\lambda_{np}}, & \text{if } n = K+1 \\ b_p(n) = 0, b_{np}(n) = \frac{B_{np}}{\lambda_{np}}, & \text{if } n = K+2, \dots, N \end{cases} \quad (13)$$

where $K \in \{0, 1, \dots, N-1\}$. Parameters K , α , λ_p and λ_{np} are determined as follows.

$$G(d(K+1)) \leq K \leq G(d(K)) \quad (14)$$

with $G(v) = N \frac{v}{(1+v)}$ for $v \geq 0$, and:

$$\lambda_p = \max(G(d(K+1)), K), \quad (15)$$

$$\lambda_{np} = N - \lambda_p, \quad (16)$$

$$\alpha = \lambda_p - K. \quad (17)$$

Recall that from Equation 5, we always have $b(l, m, n) \geq 0$. Thus, Equation 13 indicates that when $b_{np}(n) = 0$, the first K users are scheduled in the protected resources; likewise, when $b_p(n) = 0$, the users $n = K+2, \dots, N$ are scheduled in the non-protected resources. Only the $(K+1)$ th user can be scheduled in both the protected and non-protected resources if $0 < \alpha < 1$, or the $(K+1)$ th user can be placed to either of the two types of resources by setting $\alpha = 0$ or $\alpha = 1$.

As mentioned in Section 3, we consider a BS with 3 sectors. Recall that three different types of users need to be identified in order to apply the scheduling restrictions. In our study, we apply pairwise comparison between BS sectors by using the methods briefed above to identify the three types of users. As an example, let us consider sector 1, and suppose N_1 devices are served by it. For an arbitrary device q_{n_1} , $n_1 \in \{1, 2, \dots, N_1\}$ served by sector 1, we apply the aforementioned methods twice and compare sector 1 with sector 2 and sector 3 alternatively. If in both cases q_{n_1} is identified to be scheduled in non-protected resources of sector 1, then q_{n_1} is classified as a type 1 user. If in both cases q_{n_1} is identified to be scheduled in protected resources of sector 2 and sector 3, then q_{n_1} is a type 3 user. The rest of the users (if any) are type 2 users that have either sector 2 or sector 3 as their dominant interferer.

5 Multi-antenna solutions for backhaul links of MNs

Beside the time domain methods, we can also use multi-antenna solutions to improve the received signal quality at the backhaul links of MNs. One of the benefits of using MNs is that public transportation vehicles are less constrained by antenna array size or power compared to regular UEs. Thus, more antenna elements and more advanced signal processing algorithms can be employed. In this study, we consider a single antenna at each sector of the macro BS, and multiple antennas are used for the backhaul link reception at the MNs. The idea of using multiple receiving antennas in wireless communication systems has a long history ([54] Ch. 20). In practice, depending on whether CSI from the interferers can be obtained, different schemes can be applied to improve the received SINR ([54] Ch. 20). In this study, we consider two cases, i.e., maximum ratio combining (MRC), and SINR maximization by interference suppression.

5.1 Maximum ratio combining

If only the CSI of the desired signal can be estimated at each of the antennas at the receiver, MRC can be used to combine the desired signal from each antenna at the receiver constructively to maximize the desired signal power. An MRC receiver is optimal in terms of SNR, i.e., it maximizes the output power of the received desired signal [55]. The received signal consists of the desired signal, interference signal, and thermal noise. Suppose the receiver is equipped with p antennas. In a frequency flat-fading case, e.g., within a PRB, at time k , if we have N_L interferers, the received signal can be expressed as:

$$\mathbf{y}_k = \mathbf{h}_k x_k + \sum_{j=1}^{N_L} \mathbf{h}_{j,k} x_{j,k} + \mathbf{n}_k, \quad (18)$$

where \mathbf{y} is a $p \times 1$ column vector that contains the received signal at each antenna, x_k is the desired signal, and $x_{j,k}$ is the interfering signal from the j th interferer. Moreover, \mathbf{h}_k and $\mathbf{h}_{j,k}$ represent the desired and j th interfering signal propagation vectors, respectively, and \mathbf{n}_k is the thermal noise. We assume that the desired signal and interfering signals are uncorrelated.

At the receiver, let \mathbf{w}_k be a vector that contains the weight applied at each antenna at time k . Then, the combined signal at the MN is given by:

$$\mathbf{z}_k = \mathbf{w}_k^H \mathbf{y}_k = \mathbf{w}_k^H \mathbf{h}_k x_k + \sum_{j=1}^{N_L} \mathbf{w}_k^H \mathbf{h}_{j,k} x_{j,k} + \mathbf{w}_k^H \mathbf{n}_k, \quad (19)$$

where $(\cdot)^H$ denotes the complex conjugate transpose. The MRC solution that maximizes the desired signal power

uses the combining weights as $\mathbf{w}_k^* = \mathbf{h}_k$, which yields the following instantaneous output SINR at the MN:

$$\gamma_k = \frac{|\mathbf{h}_k^H \mathbf{h}_k|^2}{\left| \sum_{j=1}^L \mathbf{h}_k^H \mathbf{h}_{j,k} x_{j,k} + \mathbf{h}_k^H \mathbf{n}_k \right|^2}. \quad (20)$$

From Equation 20, we can observe that, although at a given time the output power of the desired signal is maximized, the SINR is not maximized due to the presence of the interfering signal. However, if no CSI from the interferers can be obtained, MRC is the optimal solution to maximize the received desired signal power.

5.2 SINR maximization by interference suppression

As mentioned before, MRC combining is optimal in terms of SNR; however, we can do better if the phase and amplitude of the interferers can also be estimated. If CSI from the interferers can be obtained, we can exploit the multiple antennas at the receiver to suppress the interference signals, and thereby maximize the output SINR. This scheme falls into the category of interference rejection combining (IRC) [56]([57] Ch. 10).

From Equation 19, we can obtain the received SINR with some arbitrary weight vector \mathbf{w}_k as:

$$\gamma_k = \frac{\mathbf{w}_k^H \mathbf{h}_k \mathbf{h}_k^H \mathbf{w}_k}{\mathbf{w}_k^H \left(\sum_{j=1}^L \mathbf{h}_{j,k} \mathbf{h}_{j,k}^H + \mathbf{R} \right) \mathbf{w}_k}, \quad (21)$$

where \mathbf{R} is the noise covariance for the receiver antennas, same for all k . Thus, if we know $\mathbf{h}_{j,k}$, we can obtain the optimal weight that maximizes the SINR by solving:

$$\mathbf{w}_k^* = \arg \max_{\mathbf{w}_k} \frac{\mathbf{w}_k^H \mathbf{h}_k \mathbf{h}_k^H \mathbf{w}_k}{\mathbf{w}_k^H \left(\sum_{j=1}^L \mathbf{h}_{j,k} \mathbf{h}_{j,k}^H + \mathbf{R} \right) \mathbf{w}_k}. \quad (22)$$

The optimal weight problem (22) is a generalized eigenvalue problem, and the optimal weight is given as [56]:

$$\mathbf{w}_k^* = \text{EIG}_{\max} \left(\left(\sum_{j=1}^L \mathbf{h}_{j,k} \mathbf{h}_{j,k}^H + \mathbf{R} \right)^{-1} \mathbf{h}_k \mathbf{h}_k^H \right), \quad (23)$$

where $\text{EIG}_{\max}(\cdot)$ denotes the dominant eigenvector of a matrix \mathbf{e} , and we assume that antenna noise is independent among the antenna elements, i.e., $\mathbf{R} = \sigma_n^2 \mathbf{I}_{p \times p}$, where σ_n^2 is the noise power at each antenna, and $\mathbf{I}_{p \times p}$ is the identity matrix of size p .

As an example, Figure 6 compares the cdf of SINR at the backhaul links of MNs. As we can see from the figure, the IRC gives the best result as expected, since it maximizes the SINR. Regarding the use of ABSs and MRC, compared to the case without using any ICIC scheme, the SINR at the receiver is also improved. The MRC scheme improves the performance in the low SINR region, but since MRC cannot remove the interference, in an interference limited scenario, the general performance of it is not as good as the other two schemes. Section 7 provides more detailed system level evaluation results.

6 Interference coordination for access links of MNs

Since the access links of MNs are operating at the same frequency bands as the micro cells, as discussed in Section 3.1, the access links need to be protected in order to accommodate the traffic from their backhaul links. We

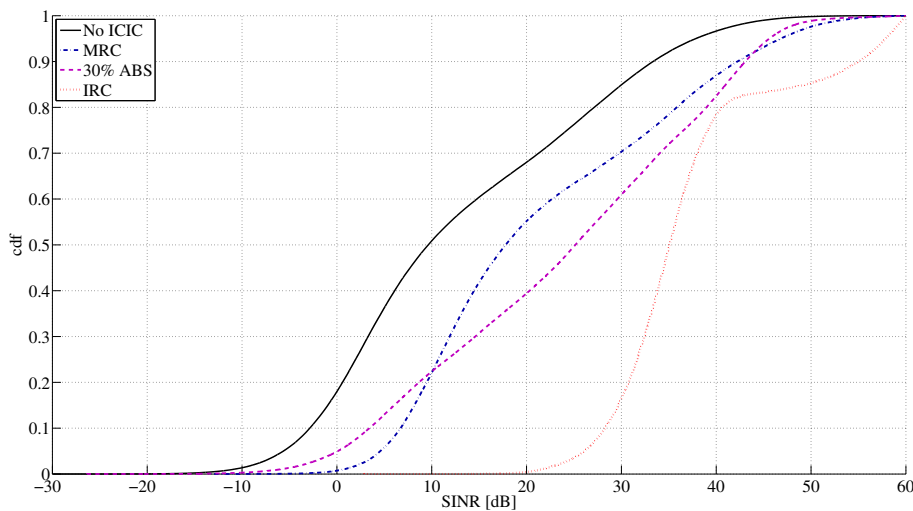


Figure 6 The cdf of SINR per PRB of the backhaul links of MNs. For MRC and IRC, four antennas are used at the receiver. The detailed parameters used for this plot are given in Section 7. The solid black line is the SINR when no ICIC schemes are used. The dash-dot blue line is the SINR when MRC is used. The dashed purple line is the SINR when the number of ABSs is 30% at the macro sectors. The dotted red link is the SINR when IRC is used.

consider to configure ABSs at the micro cells to alleviate the interference problem that they cause to the access links of MNs. There are two ways to configure the ABS patterns for the micro cells: 1) each micro cell configures its own ABS pattern, or 2) the micro cells in a given area use the same ABS pattern. Recall that rather than maximizing the throughput of the access links, our goal is to protect the access links of MNs, and thereby the traffic from their backhaul links can be accommodated. Therefore, we just need to configure a minimum number of ABSs to ensure that the access links of MNs can successfully convey the traffic from their backhaul links. However, as mentioned in Section 4.1, the ABS patterns can only be updated in a semi-static pattern. The criteria of configuring ABS patterns should be based on an average throughput (e.g., one or several ABS duty cycles), rather than the instantaneous throughput of each of the links. This is reasonable, as we can assume an MN can buffer the data from its backhaul link. As long as the buffer is big enough, the access link does not need to instantly accommodate the traffic from its backhaul link. Moreover, we can also optimize the density and ABS patterns to minimize the end-to-end transmission delays.

Furthermore, while a public transportation vehicle is moving, it can pass through several micro cells in a fairly short time. As discussed in [22,23], the typical updating time of ABS configurations is in the order of minutes, and therefore it is reasonable to assume that the same ABS configuration will be used by several micro cells in a given area. In this way, not only the signaling overhead to communicate the ABS configurations between different nodes can be reduced, but also the measurement and feedback from the MNs to the network can be less frequent. Hence, in this study, we use the same ABSs pattern for all the micro cells in the area given in Figure 1.

We consider the average throughput over N_{sf} subframes, where N_{sf} is the number of total subframes in one or several ABSs duty cycles. Our object is to configure a minimum number of ABSs in these N_{sf} subframes, such that the access links of MNs can successfully convey the traffic from their backhaul links. Let $\mathcal{I}_i \in \{0, 1\}$, $i = 1, 2, 3 \dots N_{sf}$ indicate the status of the ABSs, where $\mathcal{I}_i = 0$ indicates the i th subframe is configured to be an ABS, and $\mathcal{I}_i = 1$ indicates the i th subframe is not configured to be an ABS. Therefore, for each subframe, depending whether it is configured as one of the ABSs by the micro cells, two different rates can be observed at each MN. Let $r_{0,i}(\nu)$ be the throughput of the access link of the ν th MN when the i th subframe is configured as ABS, and $r_{1,i}(\nu)$ be the throughput of the access link of the ν th MN when the i th subframe is not configured as ABS. Then, we can formulate the optimization problem as:

$$\begin{aligned} & \max \sum_{i=1}^{N_{sf}} \mathcal{I}_i \\ & \text{subject to} \\ & \sum_{i=1}^{N_{sf}} (1 - \mathcal{I}_i) r_{0,i}(\nu) + \mathcal{I}_i r_{1,i}(\nu) \geq \bar{R}(\nu), \quad (24) \end{aligned}$$

where $\bar{R}(\nu)$ is the average throughput of the backhaul link of the ν th MN during N_{sf} subframes. Problem (24) is an integer linear programming problem, and if $r_{0,i}(\nu)$, $r_{1,i}(\nu)$ and $\bar{R}(\nu)$ are known, the solution of problem 24 can be easily found ([58] Ch. 11).

However, in practice $\bar{R}(\nu)$ cannot be obtained beforehand, and $r_{0,i}(\nu)$, $r_{1,i}(\nu)$ cannot even be observed due to the randomness of wireless channels, measurement restrictions, and feedback delays. Thus, in this study, a reinforcement-learning approach [59] is adopted to configure the ABS patterns for the micro cells. The main idea is that we assume VUEs are primary users, and a set of ABS patterns is pre-defined for the micro cells. Our goal is to minimize the number of ABSs used by the micro BSs in a given area and satisfy the average throughput requirement for the access link of the worst MN in that area.

First, the micro BSs in a given area choose a configuration from the pre-defined set of ABSs patterns^f, and collect feedback from the MNs in that area according to this setting. If during the measurement time, e.g., one or several ABSs duty cycles, this setting cannot satisfy the average throughput of the access link of the worst MN in that area, then the micro BSs choose a new ABSs pattern that offers more protection. Otherwise, the micro BSs can lower the number of ABSs until it reaches the minimum number that satisfy the average throughput of the access link of the worst MN in that area. Recall that we assume MNs can buffer the data from their backhaul links. Therefore, as long as the buffer is big enough, the initial value of ABSs pattern is reasonable, and the measurement time is relatively short, there are no concerns about unnecessary drop of packets and excessive end-to-end delays.

The algorithm used in this evaluation is summarized in Algorithm 1. In practice, step 3 in Algorithm 1 may be optional, as it only ensures that the number of ABSs is not set too high at the micro cells. For example, due to the sudden increase in the number of MNs during rush hours, more ABSs may be allocated by the micro cells, and after the rush hours when the number of MNs drops in a given area, we may need to lower the number of ABSs in order not to waste the resources at the micro cells. This can also be achieved by using a timer at the micro cells, which will lower the number of ABSs after a given time. We emphasize that the configuration of ABSs should not be frequent, at least not in the order of several seconds.

Thus, in practice, a small margin may be added to the minimum number of ABSs to accommodate the sudden change of the number of vehicles or the propagation conditions. In a larger time scale, i.e., in an order of several minutes or even hours, the micro BSs in the given area can update the configuration of ABS patterns according to the feedback from the MNs.

Algorithm 1 Configuration of the number of ABSs for the micro BSs

Step 1 Initialize the ABS configuration

- 1: Index all the possible ABSs configurations in ascending orders according to the number of ABSs.
- 2: Set all the micro BSs to use the configuration with the minimum number of ABSs.

Step 2 Update the ABS configurations

- 1: All the MNs in the given area feed back the measurement of their average access link throughput to the network.
- 2: **if** one of the MNs reports is insufficient in capacity, **then**
- 3: The network identifies the index of the ABS configuration with minimum increase of the ABSs, and inform the micro BSs to update their ABSs settings.
- 4: **else**
- 5: The micro BSs keep using the previous ABS configuration.
- 6: **end if**

Step 3 Re-configure the ABSs configurations (optional)

- 1: **if** none of the MNs report is insufficient in number of ABSs after some minutes, **then**
 - 2: Set all the micro BSs to use the configuration with the minimum number of ABSs.
 - 3: Repeat step 2.
 - 4: **end if**
-

7 Performance evaluation

In this section, we compare and evaluate the MN interference techniques and discussed in earlier sections, through system level simulations. A semi-static drop based approach is adopted. The simulation area is shown in Figure 1. According to calibration setups given in METIS simulation assumptions ([14] Table 3.7), we consider that macro and micro BSs are operating on different frequency bands, with different bandwidths. To help compare different technical solutions, METIS provides implementations of the path-loss and shadowing channel models for the macro and micro sectors [14].^g The METIS path-loss and shadowing modeling is based on ray

tracing and takes into account the positions of the BSs and the geometry of the Madrid grid to ensure correct spatial property of the channels. Therefore, as long as the position and the antenna height of a receiver are determined, its path-loss and shadowing are also determined. As suggested by METIS, the small scale fading coefficients are generated according to the ITU-R urban macro cell (UMa) and urban micro cell (UMi) channel models for the macro and micro sectors, respectively [14].

To ensure the correct statistical properties of the small scale fading coefficients, all the channel coefficients are generated and normalized at the beginning of each drop. The coherence time of the channel is based on the Doppler spectrum of the receivers according to their velocities. A grid-based geometry is set in the ITU-R channel models to ensure the proper coherence bandwidth. Detailed descriptions of the ITU-R UMa and UMi channel models are given in [60].^h A non-line-of-sight (NLOS) propagation condition is considered for the macro sectors, and for the micro sectors line-of-sight (LOS) propagation is considered if the receivers are on the same street as the transmitters, otherwise the channel is considered to be NLOS. The propagation of the interference signals between the access links of MNs are modeled in the same way as the micro cells, but with an antenna height of 3.5 m. Because of the size of the public transportation vehicles, we assume that a fairly large space between antenna elements can be achieved. Therefore, at the backhaul receivers of the MNs, independent fading is assumed between desired signals and between the desired and interfering signals. Because a semi-static drop based simulation approach is used, the number of MNs on each street is first calculated based on the mobility model (see Table 1), and the MNs are then dropped uniformly on each street.

The VUEs are either served by macro BS sectors directly (baseline case) or via MNs that are formed by their own vehicles. Because of the estimated speed of the vehicle, and the size of the micro cells, VUEs are assumed not to be offloaded to micro cells. MNs are assumed to be using full-duplex communication with macro BS sectors and their VUEs on different frequency bands. To understand the impact of the number of VUEs on board, in addition to the case of dropping VUEs uniformly on each vehicle with $i_v \sim \mathcal{U}(1, 50)$, we also consider a case when each vehicle has a fixed number of 25 VUEs on board. The expected total number of users, i.e., VUEs, macro UEs, and micro UEs is kept the same for all cases. In the simulation, for each case, 850 drops are conducted with 40 sub-frames in each drop. The channel realizations and the positions of MNs and UEs are updated on a drop basis. The detailed parameters are summarized in Table 1 [14], and the detailed ABS configurations are given in the appendix.

Table 1 Simulation parameters

Component	Configuration parameters
Buildings and streets	Nine buildings 120 by 120 m with six floors (3.5 m height of each floor), see Figure 1. Road width 21 m (including sidewalks and parking lanes)
Macro BS	Height: 5 m above the top of the middle building (see Figure 1) Maximum transmit power (per 10 MHz): 43 dBm Carrier: 800 MHz Bandwidth: 20 MHz Antenna configuration: 17 dBi gain, three sectors (one antenna per sector), 0°, 120°, and 240° with respect to the north
Micro BS	Height: 10 m above the ground close to middle point of south and east walls Positions: see Figure 1 Maximum transmit power (per 10 MHz): 30 dBm Carrier: 2.6 GHz Bandwidth: 80 MHz Cell range expansion bias: 5 dB Antenna configuration: 17 dBi gain, two sectors (one antenna per sector), pointing to the main street with an angle of 20° with respect to the closest wall
Moving network	Full-duplex Speed: 50 km/h Height: 3.5 m above the ground Mobility model: public transportation vehicles enter each street through a Poisson process with an inter-arrival time of 2 min Maximum transmit power indoor (per 10 MHz): 10 dBm Carrier: 800 MHz for backhaul links, and 2.6 GHz for access links Bandwidth: 20 MHz for backhaul links and 80 MHz for access links Antenna configuration both indoor and outdoor: single antenna, 0 dBi gain omnidirectional antenna Receiver noise figure: 5 dB
Outdoor UEs (macro UE, micro UE)	Speed: 0 to 3 km/h Height: 1.5 m above the ground Positions: uniformly randomly dropped, 50 UEs per road Cell selection: based on received power with 5 dB CRE bias for micro cells Receiver noise figure: 9 dB
VUEs	Height: 1.5 m above the ground Position: uniformly randomly dropped inside a vehicle Number of VUEs in each vehicle: 1) uniformly from the interval [1, 50]; 2) 25 VUEs per vehicle Cell selection: 1) same as macro UEs (baseline case); 2) always connect to the MN of their own vehicles (other cases) Receiver noise figure: 9 dB

A full-buffer traffic model is considered, and the end user throughput is our metric. The throughput, for the backhaul links of MNs and end users, is calculated based on a look-up table method according to the instantaneous received SINR [50] assuming all the information

bits are correctly decoded. Moreover, we also follow the constraints of the current LTE-A systems in terms of scheduling, link adaptation, and modulation and coding schemes.¹ Details of the considered simulation implementations can be found in, for example, [50]. In the following,

first, throughput performance of macro UEs and VUEs will be investigated, followed by the throughput simulations of micro UEs.

7.1 Performance analysis for macro UEs and VUEs

VUEs are served directly by the macro BSs in the baseline case, and via MNs for the other cases. An MN is regarded as a super user that communicates with macro BS sectors and aggregates traffic for its VUEs. In the cases when ABSs are configured at the macro sectors, the same scheduling restrictions and protections are applied for both the backhaul links of MNs and macro UEs, and a single antenna is assumed for all transmitters and receivers. For other cases, only the receivers of MN backhaul links are assumed to be equipped with multiple antennas, and no combination using ABSs together with multi-antennas is considered. The detailed scheduling and resource allocation methods of the macro BSs are presented in Section 4.

Figures 7, 8, 9, and 10 plot the throughput cdf of VUEs when the VPL is at 15 and 30 dB. When the VPL is 15 dB (Figures 7 and 8), we observe that compared with the baseline case, the use of MNs does not improve the throughput of VUEs, unless the IRC is used for the backhaul links of MNs. This is very sensible, because the low throughput for VUEs is mostly caused by strong interference, and the IRC scheme can effectively maximize the received SINR by suppressing the interference. The other cases cannot outperform the baseline case. There are two reasons for this: 1) by serving VUEs directly from the macro BSs, we can achieve multi-user scheduling gain (not all the VUEs are necessarily scheduled together), in addition to gains

from frequency adaptive modulations. These gains overshadow the gain of circumventing VPL using MNs (see Figure 3); 2). To minimize the signaling overhead, the current LTE-A system requires that all the PRBs allocated to a given link in one sub-frame have to use the same coding and modulation scheme ([16] Ch. 9 and 10). Under this constraint, even though the PF scheduler allocates more PRBs to the backhaul link of an MN than to a regular UE, the gain from using frequency adaptive modulation is limited. However, when the VPL is high, the benefits of using MNs are more obvious. In Figures 9 and 10, we see that all schemes outperform the baseline case for the cell edge VUEs, and the VUEs benefit the most from MNs when IRC is used for backhaul links of MNs.

Moreover, the number of VUEs on board also has an impact on the system performance. When comparing Figure 7 with Figures 8, 9, and 10, we notice some obvious differences in the throughput of the VUEs. For example, where a fixed number of 25 VUEs are on board, the 50th percentile of the VUE throughput is slightly higher than when dropping a random number of VUEs on board. This is mostly because of the scheduling decisions, because when an MN is scheduled, all its VUEs need to be scheduled at the same time. We present detailed discussion on this later in this section.

Figures 11, 12, 13, and 14 plot the throughput cdf of macro UEs when the VPL is at 15 and 30 dB. We emphasize that, by introducing MNs to the system, the performances of the macro UEs are not obviously impacted unless ABSs are used as the ICIC scheme. As expected, the macro UEs have a lower throughput when ABSs are configured, because certain sub-frames from macro BSs are

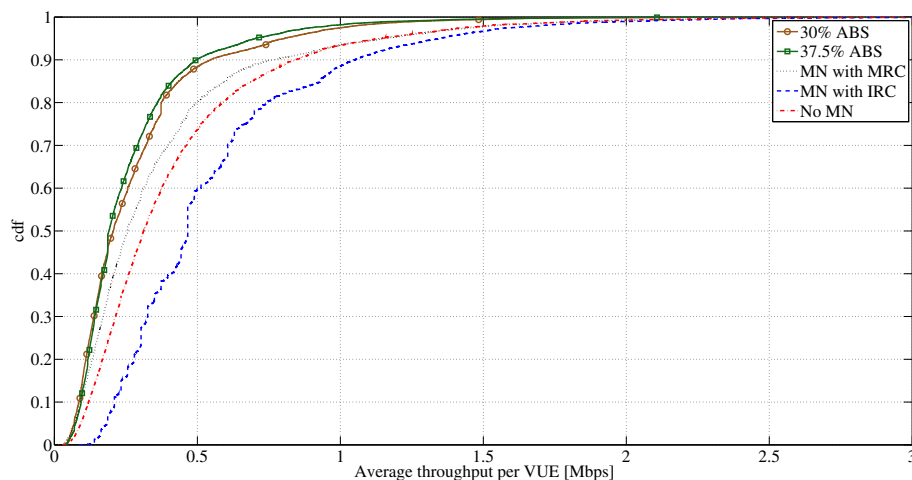


Figure 7 The cdf of VUE throughput, uniformly distributed VUEs, VPL at 15 dB. The solid green line with square markers is the average throughput per VUE when the number of ABSs is 37.5% at the macro sectors. The solid brown line with circle markers is the average throughput per VUE when the number of ABSs is 30% at the macro sectors. The dotted black line is the average throughput per VUE when MRC is used at backhaul links of MNs. The dash-dot red line is the average throughput per VUE when no MNs are used. The dashed blue line is the average throughput per VUE when IRC is used at backhaul links of MNs.

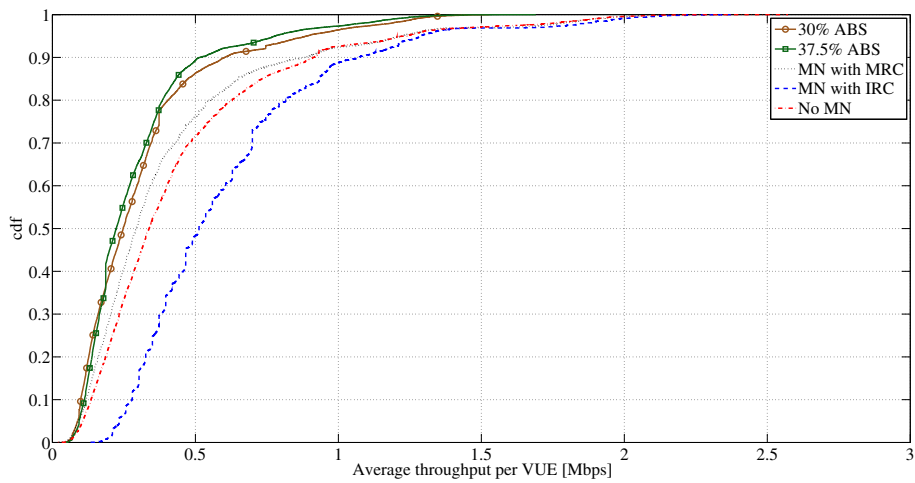


Figure 8 The cdf of VUE throughput, 25 VUEs per vehicle, VPL at 15 dB. The solid green line with square markers is the average throughput per VUE when the number of ABSs is 37.5% at the macro sectors. The solid brown line with circle markers is the average throughput per VUE when the number of ABSs is 30% at the macro sectors. The dotted black line is the average throughput per VUE when MRC is used at backhaul links of MNs. The dash-dot red line is the average throughput per VUE when no MNs are used. The dashed blue line is the average throughput per VUE when IRC is used at backhaul links of MNs.

not used. Moreover, from the figures, we observe that different VPL values have no impact on the performance of macro UEs. This is because the PF scheduler ensures the same scheduling opportunities for all the users. The number of VUEs per bus, however, has some impact on the throughput of macro UEs.

To gain a better insight into the different schemes, in Figures 15, 16, 17, and 18, we plot the 5th percentile user throughput versus the 90th percentile user throughput for the VUEs and macro UEs in all the cases. Different

schemes are differentiated by the shapes of the markers. Hollow markers represent the VUEs, and solid markers are the macro UEs. Figures 15 and 17 plot the 5th percentile versus 90th percentile user throughput for a random number of VUEs when the VPL is 15 and 30 dB, respectively. Figures 16 and 18 plot the 5th percentile versus 90th percentile user throughput for a fixed number of 25 VUEs on each vehicle, when VPL is 15 and 30 dB, respectively. In Figures 15, 16, 17, and 18, we observe that the IRC scheme gives the best performance for VUEs

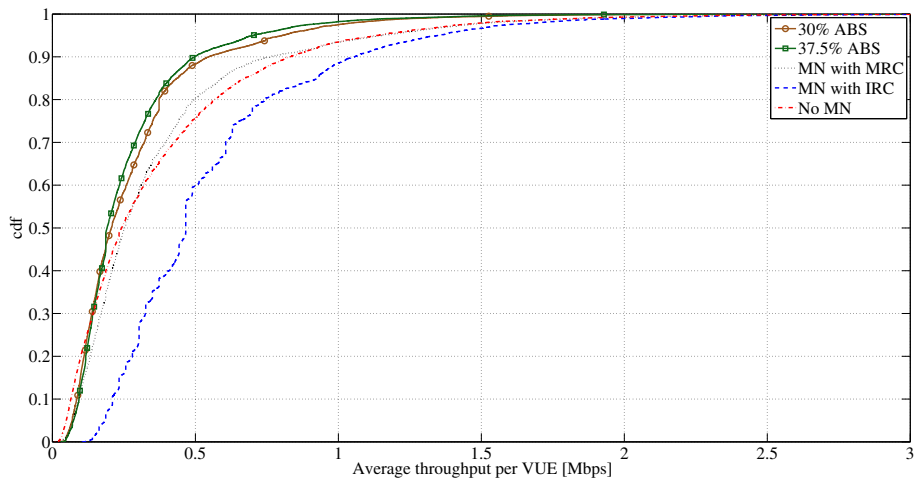


Figure 9 The cdf of VUE throughput, uniformly distributed VUEs, VPL at 30 dB. The solid green line with square markers is the average throughput per VUE when the number of ABSs is 37.5% at the macro sectors. The solid brown line with circle markers is the average throughput per VUE when the number of ABSs is 30% at the macro sectors. The dotted black line is the average throughput per VUE when MRC is used at backhaul links of MNs. The dash-dot red line is the average throughput per VUE when no MNs are used. The dashed blue line is the average throughput per VUE when IRC is used at backhaul links of MNs.

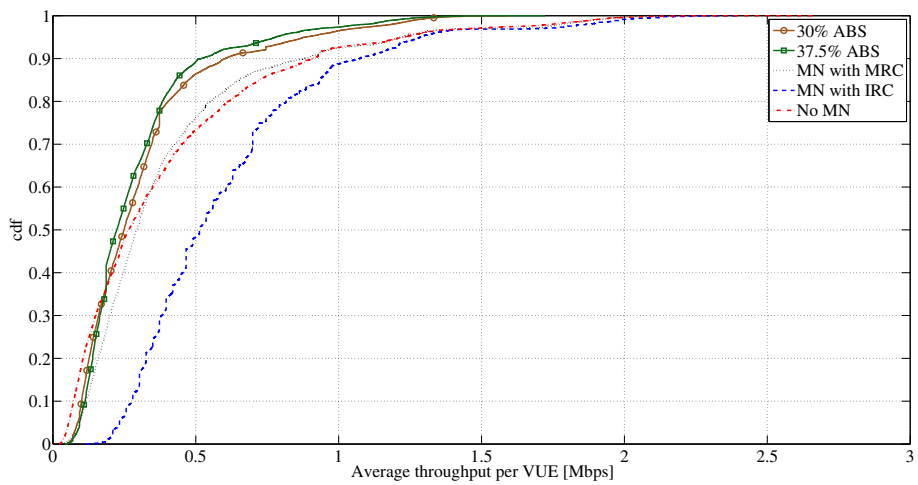


Figure 10 The cdf of VUE throughput, 25 VUEs per vehicle, VPL at 30 dB. The number of VUEs is fixed at 25 for each vehicle and VPL is at 30 dB. The solid green line with square markers is the average throughput per VUE when the number of ABSs is 37.5% at the macro sectors. The solid brown line with circle markers is the average throughput per VUE when the number of ABSs is 30% at the macro sectors. The dotted black line is the average throughput per VUE when MRC is used at backhaul links of MNs. The dash-dot red line is the average throughput per VUE when no MNs are used. The dashed blue line is the average throughput per VUE when IRC is used at backhaul links of MNs.

for all cases. Both the 5th percentile and 90th percentile throughputs have improved significantly compared with the baseline case. However, at low VPL, i.e., VPL at 15 dB, compared with the baseline case, there is no advantage for VUEs when MNs use schemes other than IRC for their backhaul links.

When the VPL increases to 30 dB, the advantage of using MNs to serve VUEs becomes obvious, because the VPL can be circumvented, and the impact of interference can be mitigated. When using MNs to serve VUEs,

depending on the ICIC schemes, compared with the baseline setup, the performance of VUEs, for either the 5th percentile or both the 5th percentile and 90th percentile throughput, is improved. The IRC gives the best performance as expected. More specifically, in the low SINR region, both the use of MRC and ABSs can improve the 5th percentile throughput of VUEs. Because ABSs are used to mute certain sub-frames from the macro cells to protect the victim UEs, compared with the baseline case, there is an obvious improvement in the 5th percentile

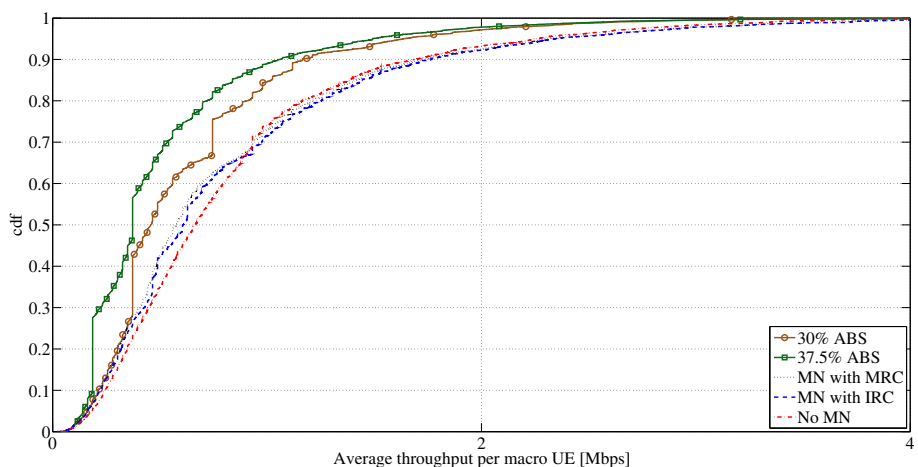


Figure 11 The cdf of macro UE throughput, uniformly distributed VUEs, VPL at 15 dB. The solid green line with square markers is the average throughput per VUE when the number of ABSs is 37.5% at the macro sectors. The solid brown line with circle markers is the average throughput per VUE when the number of ABSs is 30% at the macro sectors. The dotted black line is the average throughput per VUE when MRC is used at backhaul links of MNs. The dash-dot red line is the average throughput per VUE when no MNs are used. The dashed blue line is the average throughput per VUE when IRC is used at backhaul links of MNs.

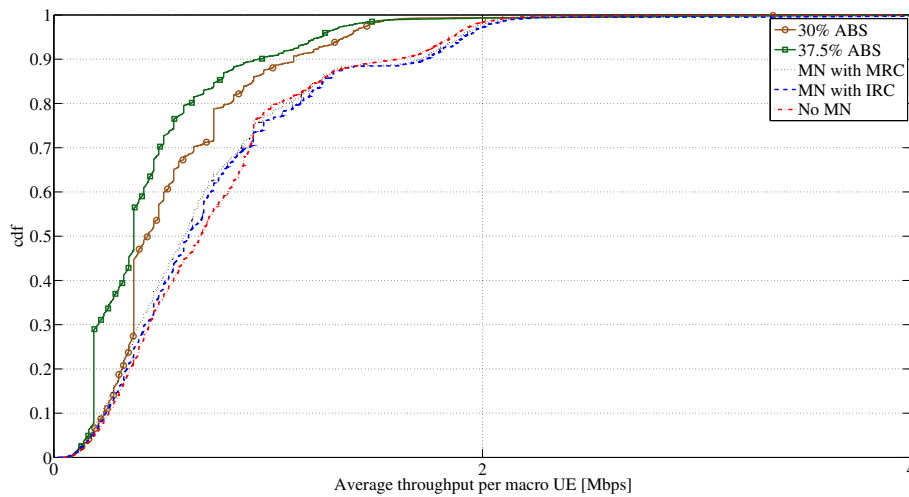


Figure 12 The cdf of macro UE throughput, 25 VUEs per vehicle, VPL at 15 dB. The solid green line with square markers is the average throughput per VUE when the number of ABSs is 37.5% at the macro sectors. The solid brown line with circle markers is the average throughput per VUE when the number of ABSs is 30% at the macro sectors. The dotted black line is the average throughput per VUE when MRC is used at backhaul links of MNs. The dash-dot red line is the average throughput per VUE when no MNs are used. The dashed blue line is the average throughput per VUE when IRC is used at backhaul links of MNs.

throughput of the VUEs, but a lower throughput at the high SINR regions, as expected, and, as also expected, the IRC gives the best performance for both the 5th percentile and 90th percentile throughput of the VUEs.

Furthermore, the number of VUEs on board affects the user throughput. Because an MN is regarded as a super user that aggregates the traffic of its VUEs, if an MN is scheduled, the PRBs allocated to its backhaul link are proportional to the number of VUEs it serves. Therefore, the PF scheduler has less scheduling flexibility. The

inflexibility can be easily observed from the cdf plots of the throughput of macro UEs. When comparing Figure 11 with Figures 12, 13, and 14, we observe that the cdf curves are less smooth when there is a fixed number of 25 VUEs on board. From Figures 15, 16, 17, and 18, we observe that even though the total expected number of VUEs in the system is the same, compared with the random VUEs per vehicle, if we have a fixed number of 25 VUEs per vehicle, the 5th percentile of the VUE throughput increases for all the cases when the VUEs are served by the MNs. But

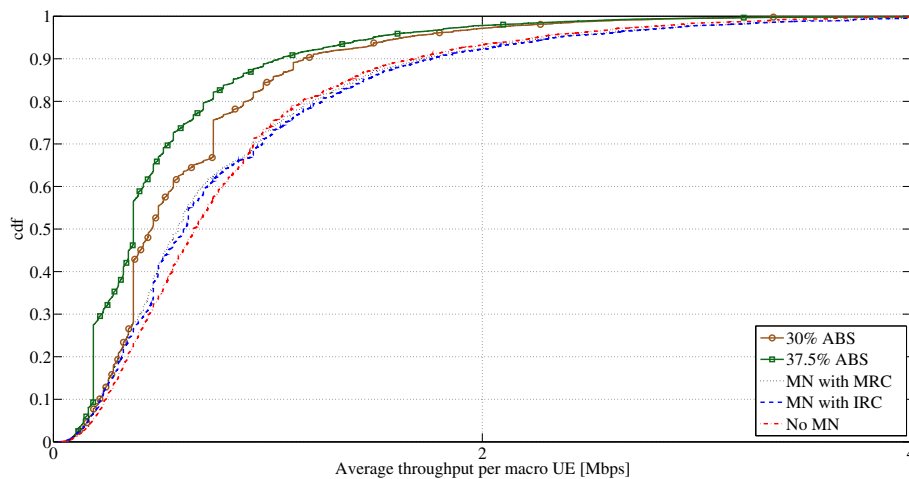


Figure 13 The cdf of macro UE throughput, uniformly distributed VUEs, VPL at 30 dB. The solid green line with square markers is the average throughput per VUE when the number of ABSs is 37.5% at the macro sectors. The solid brown line with circle markers is the average throughput per VUE when the number of ABSs is 30% at the macro sectors. The dotted black line is the average throughput per VUE when MRC is used at backhaul links of MNs. The dash-dot red line is the average throughput per VUE when no MNs are used. The dashed blue line is the average throughput per VUE when IRC is used at backhaul links of MNs.

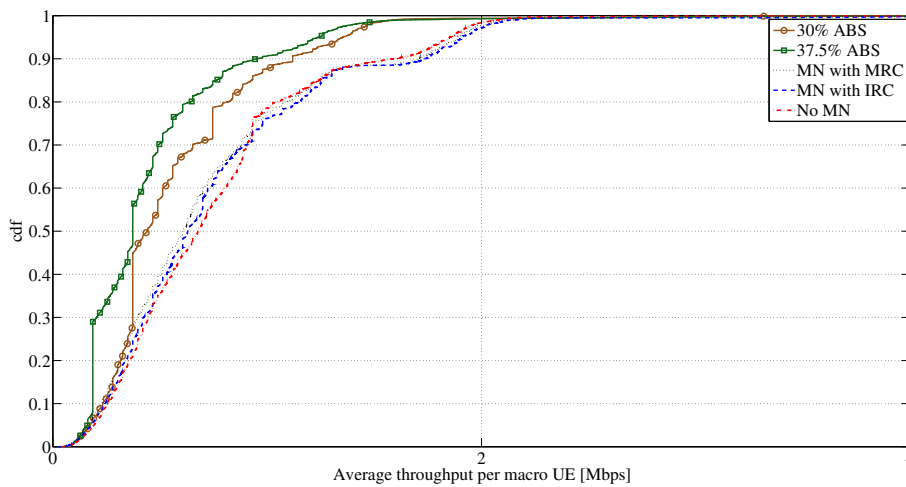


Figure 14 The cdf of macro UE throughput, 25 VUEs per vehicle, VPL at 30 dB. The solid green line with square markers is the average throughput per VUE when the number of ABSs is 37.5% at the macro sectors. The solid brown line with circle markers is the average throughput per VUE when the number of ABSs is 30% at the macro sectors. The dotted black line is the average throughput per VUE when MRC is used at backhaul links of MNs. The dash-dot red line is the average throughput per VUE when no MNs are used. The dashed blue line is the average throughput per VUE when IRC is used at backhaul links of MNs.

this is at a cost of slightly lowering the throughput of the macro UEs.

7.2 Performance analysis for micro UEs

We configure ABSs for the micro BSs to protect the access links of MNs from the interference caused by the micro BS sectors. Figures 19, 20, 21, and 22 plot the throughput

cdfs of the micro UEs. Compared with the baseline case, i.e., VUEs served directly via macro BSs, there is a slight degradation in the micro UE throughput in the presence of MNs. This is because when using ABSs, some subframes of the micro BSs are not employed. When the VPL is 15 dB (Figures 19 and 20), the ICIC schemes that offer higher throughput at the backhaul links of MNs have a

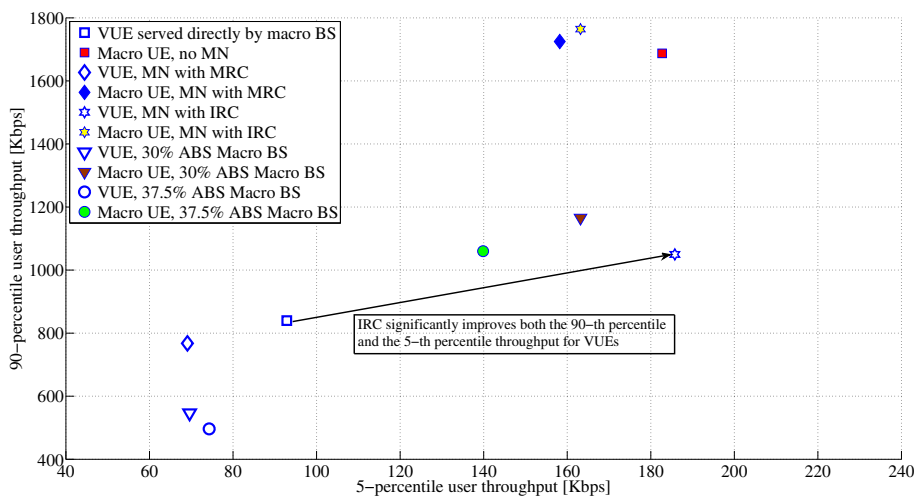


Figure 15 5th percentile vs 90th percentile user throughput for macro UEs and VUEs, uniformly distributed VUEs, VPL at 15 dB. The hollow square marker is the VUE throughput when they are served directly by the macro BS. The solid red square marker is the macro UE throughput when there is no MNs in the system. The hollow diamond marker is the VUE throughput when MRC is used at the backhaul links of MNs. The solid diamond blue marker is the macro UE throughput when MRC is used at the backhaul links of MNs. The hollow star marker is the VUE throughput when IRC is used at the backhaul links of MNs. The solid star yellow marker is the macro UE throughput when IRC is used at the backhaul links of MNs. The hollow triangle marker is the VUE throughput when the number of ABSs is 30% at the macro BS. The solid triangle brown marker is the macro UE throughput when the number of ABSs is 30% at the macro BS. The hollow circle marker is the VUE throughput when the number of ABSs is 37.5% at the macro BS. The solid circle green marker is the macro UE throughput when the number of ABSs is 37.5% at the macro BS.

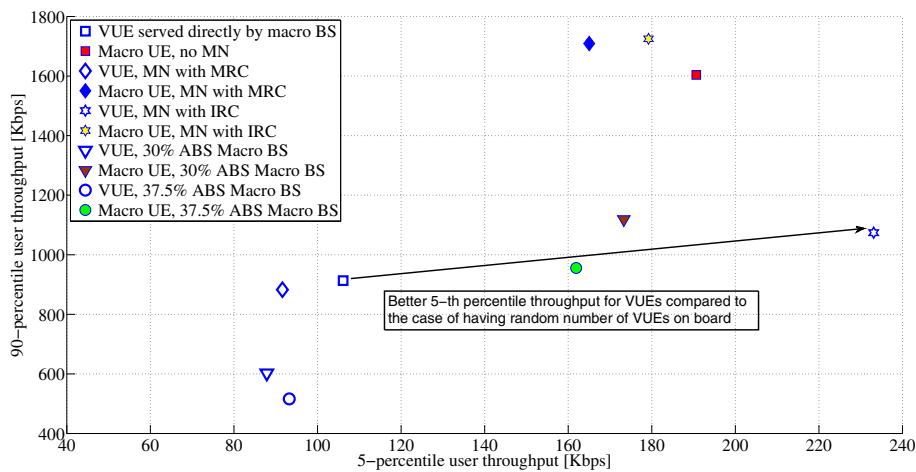


Figure 16 5th percentile vs 90th percentile user throughput for macro UEs and VUEs, 25 VUEs per vehicle, VPL at 15 dB. The hollow square marker is the VUE throughput when they are served directly by the macro BS. The solid red square marker is the macro UE throughput when there is no MNs in the system. The hollow diamond marker is the VUE throughput when MRC is used at the backhaul links of MNs. The solid diamond blue marker is the macro UE throughput when MRC is used at the backhaul links of MNs. The hollow star marker is the VUE throughput when IRC is used at the backhaul links of MNs. The solid star yellow marker is the macro UE throughput when IRC is used at the backhaul links of MNs. The hollow triangle marker is the VUE throughput when the number of ABSs is 30% at the macro BS. The solid triangle brown marker is the macro UE throughput when the number of ABSs is 30% at the macro BS. The hollow circle marker is the VUE throughput when the number of ABSs is 37.5% at the macro BS. The solid circle green marker is the macro UE throughput when the number of ABSs is 37.5% at the macro BS.

greater impact on the throughput of micro UEs. This is because more ABSs are needed for the micro BSs to protect the access links of MNs to accommodate the traffic from their backhaul links. The impact, however, is not very obvious because of the relatively large bandwidth of the micro cells.

When the VPL is at 30 dB (Figures 21 and 22), compared with the baseline case, when the MNs are introduced to the system, there is still a slight degradation in micro UE throughput but not as obvious as when the VPL is at 15 dB. There are two reasons for this. First, the interference power from micro BSs to the access links of MNs can be

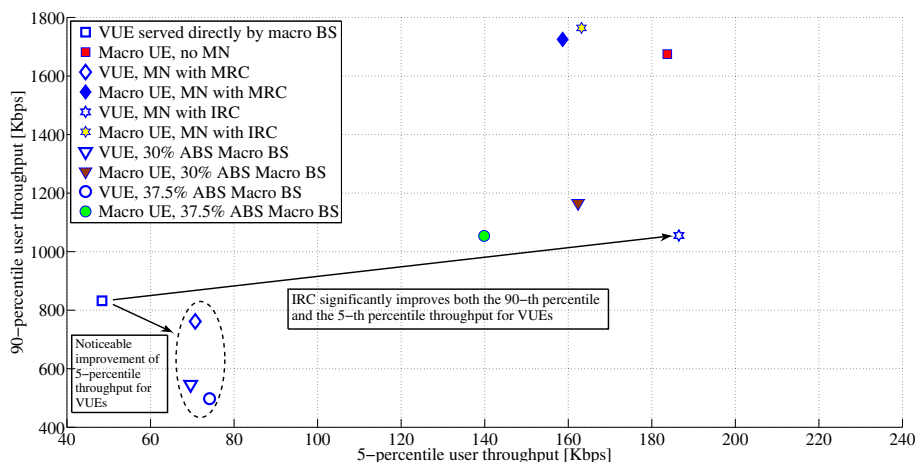


Figure 17 5th percentile vs 90th percentile user throughput for macro UEs and VUEs, uniformly distributed VUEs, VPL at 30 dB. The hollow square marker is the VUE throughput when they are served directly by the macro BS. The solid red square marker is the macro UE throughput when there is no MNs in the system. The hollow diamond marker is the VUE throughput when MRC is used at the backhaul links of MNs. The solid diamond blue marker is the macro UE throughput when MRC is used at the backhaul links of MNs. The hollow star marker is the VUE throughput when IRC is used at the backhaul links of MNs. The solid star yellow marker is the macro UE throughput when IRC is used at the backhaul links of MNs. The hollow triangle marker is the VUE throughput when the number of ABSs is 30% at the macro BS. The solid triangle brown marker is the macro UE throughput when the number of ABSs is 30% at the macro BS. The hollow circle marker is the VUE throughput when the number of ABSs is 37.5% at the macro BS. The solid circle green marker is the macro UE throughput when the number of ABSs is 37.5% at the macro BS.

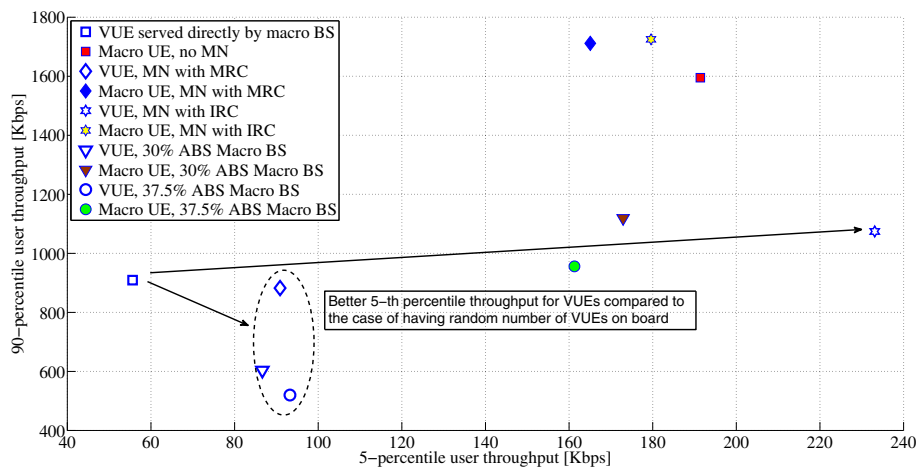


Figure 18 5th percentile vs 90th percentile user throughput for macro UEs and VUEs, 25 VUEs per vehicle, VPL at 30 dB. The hollow square marker is the VUE throughput when they are served directly by the macro BS. The solid red square marker is the macro UE throughput when there is no MNs in the system. The hollow diamond marker is the VUE throughput when MRC is used at the backhaul links of MNs. The solid diamond blue marker is the macro UE throughput when MRC is used at the backhaul links of MNs. The hollow star marker is the VUE throughput when IRC is used at the backhaul links of MNs. The solid star yellow marker is the macro UE throughput when IRC is used at the backhaul links of MNs. The hollow triangle marker is the VUE throughput when the number of ABSs is 30% at the macro BS. The solid triangle brown marker is the macro UE throughput when the number of ABSs is 30% at the macro BS. The hollow circle marker is the VUE throughput when the number of ABSs is 37.5% at the macro BS. The solid circle green marker is the macro UE throughput when the number of ABSs is 37.5% at the macro BS.

significantly attenuated by the vehicles. Therefore, fewer ABSs are required for the micro BSs to protect the access links of MNs. Second, at high VPL, the interference from the access links of MNs to nearby micro UEs (see Figure 2) can also be attenuated by the vehicles.

Moreover, at 30 dB VPL, we observe that the considered ICIC schemes used for the backhaul links of MNs have no noticeable differences with regard to the impact

on the throughput of micro UEs. This is because: 1) the vehicle can protect the access link of a MN, because the interference can be significantly attenuated by the VPL; 2) we always consider configuring the ABS patterns for the worst MN in a given area (see Section 6), and there is no noticeable difference in the required ABSs between the considered ICIC schemes. MNs offer very good link qualities to their VUEs because of the relatively short

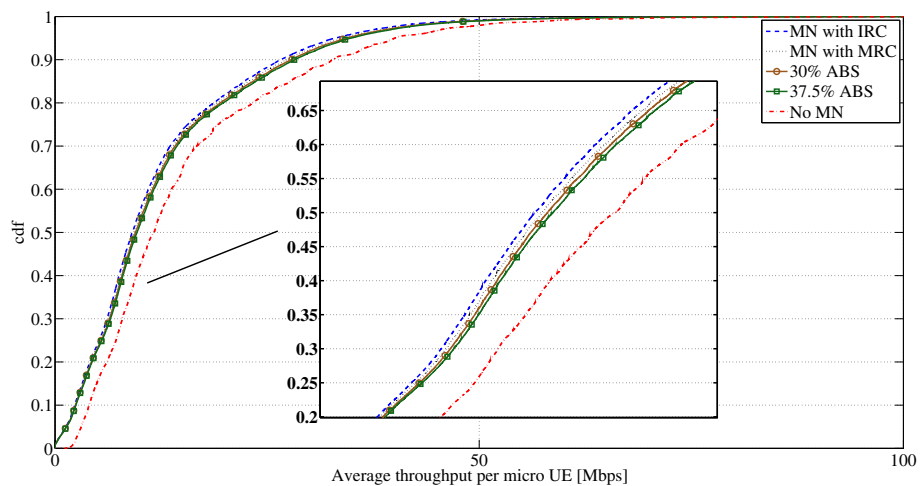


Figure 19 The cdf of micro UE throughput, uniformly distributed VUEs, VPL at 15 dB. The solid green line with square markers is the average throughput per VUE when the number of ABSs is 37.5% at the macro sectors. The solid brown line with circle markers is the average throughput per VUE when the number of ABSs is 30% at the macro sectors. The dotted black line is the average throughput per VUE when MRC is used at backhaul links of MNs. The dash-dot red line is the average throughput per VUE when no MNs are used. The dashed blue line is the average throughput per VnUE when IRC is used at backhaul links of MNs.

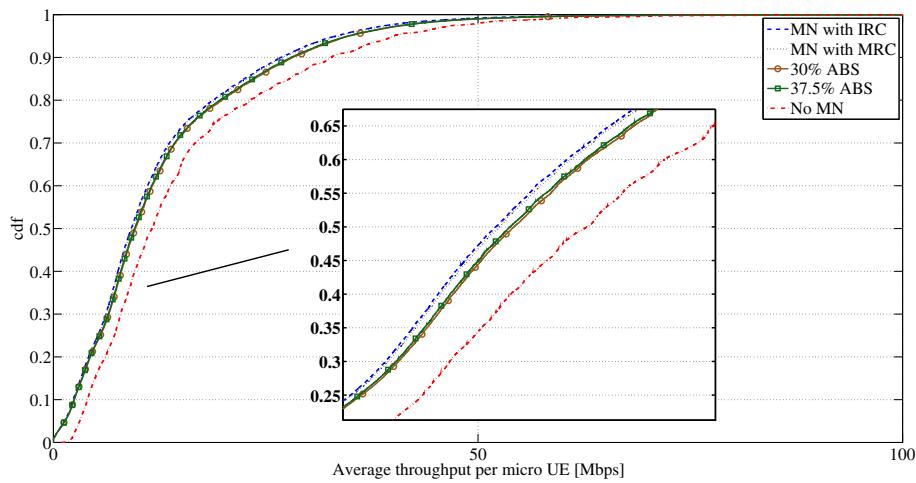


Figure 20 The cdf of micro UE throughput, 25 VUEs per vehicle, VPL at 15 dB. The solid green line with square markers is the average throughput per VUE when the number of ABSs is 37.5% at the macro sectors. The solid brown line with circle markers is the average throughput per VUE when the number of ABSs is 30% at the macro sectors. The dotted black line is the average throughput per VUE when MRC is used at backhaul links of MNs. The dash-dot red line is the average throughput per VUE when no MNs are used. The dashed blue line is the average throughput per VUE when IRC is used at backhaul links of MNs.

distance between their indoor antennas and their VUEs. Because all the micro BSs are muted at the same time, for any of the considered macro ICIC schemes, muting one sub-frame per ABSs duty cycle is sufficient for the access links of MNs to accommodate the traffic from their backhaul links. To better understand the argument above, in Table 2, we list the average ABS ratios for the different schemes. The average ABS ratio is calculated as the total number of ABSs averaged over the total

number of sub-frames in all the drops. From Table 2, we observe that when the VPL is low, more ABSs are needed from the micro cells, and the greater the backhaul throughput, the more ABSs are needed. However, when the VPL is 30 dB, only the minimum number of ABSs, i.e., one ABS per ABS duty cycle, are required for the micro cells. Unlike the macro cells, the number of VUEs on board has no observable impact on the micro UE performance.

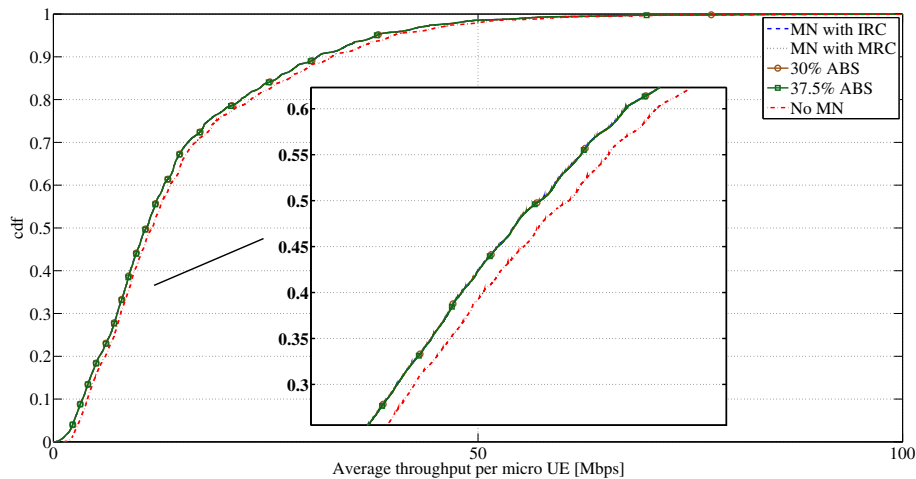


Figure 21 The cdf of micro UE throughput, uniformly distributed VUEs, VPL at 30 dB. The solid green line with square markers is the average throughput per VUE when the number of ABSs is 37.5% at the macro sectors. The solid brown line with circle markers is the average throughput per VUE when the number of ABSs is 30% at the macro sectors. The dotted black line is the average throughput per VUE when MRC is used at backhaul links of MNs. The dash-dot red line is the average throughput per VUE when no MNs are used. The dashed blue line is the average throughput per VUE when IRC is used at backhaul links of MNs.

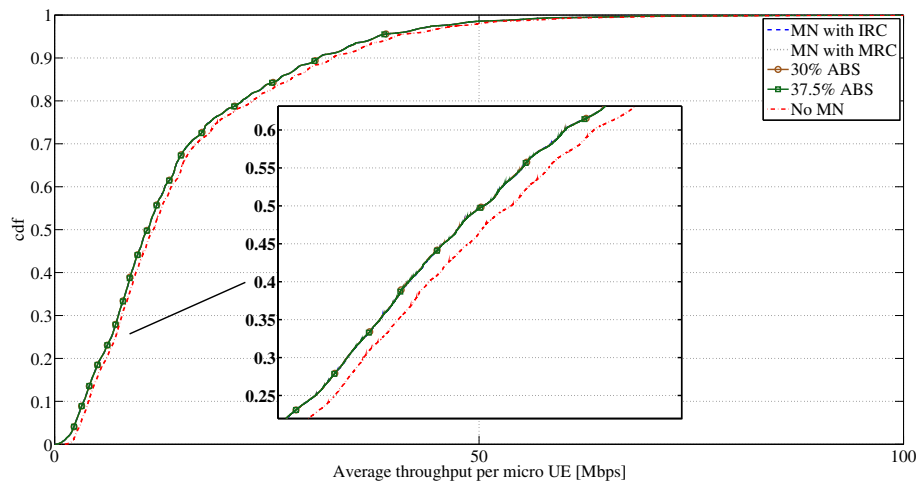


Figure 22 The cdf of micro UE throughput, 25 VUEs per vehicle, VPL at 30 dB. The solid green line with square markers is the average throughput per VUE when the number of ABSs is 37.5% at the macro sectors. The solid brown line with circle markers is the average throughput per VUE when the number of ABSs is 30% at the macro sectors. The dotted black line is the average throughput per VUE when MRC is used at backhaul links of MNs. The dash-dot red line is the average throughput per VUE when no MNs are used. The dashed blue line is the average throughput per VUE when IRC is used at backhaul links of MNs.

8 Discussion

8.1 Complexity of the considered schemes and potential impact on the current LTE-A systems

In general, when introducing MNs to current mobile communication systems, there are foreseeable impacts on both the air interference and system architecture [5,8]. Existing mobile communication systems are expected to support MNs after certain modifications. In this section, we briefly discuss the complexities of using ABSs together with scheduling restrictions for the macro sectors, using multi-antenna receivers for the MNs to enhance the backhaul link receptions, and the application of ABSs for the micro cells to protect the access links of MNs. To facilitate our discussion, we use the 3GPP Rel-12 LTE-A system as our baseline system.

As we can see from the discussion in Section 4.2, the proportional fairness based scheduling restriction is very straightforward to implement, because it only involves ordering the UEs according to their channel quality and average throughput over different protected and non-protected sub-frames. If there are n devices to be scheduled, depending on the sorting algorithm employed,

the complexity of the scheduling restriction is between $O(n \log n)$ and $O(n^2)$ ([61] Ch. 2).

However, for this scheme to work, the ABS patterns need to be exchanged between different cells, and the average throughput of a receiver over protected and non-protected sub-frames needs to be estimated. Because the current LTE-A system already supports using ABSs, the configuration of ABSs and exchange of ABS patterns between macro sectors will not introduce additional complexities to the current LTE-A system. To apply the scheduling restrictions, based on the discussion in Section 4, each macro sector needs to identify whether a receiver must be protected from one or two interferers or no protection is needed. According to Equation 9 and Equation 12, the receiver needs to feed back its average throughput when it is in both the protected and non-protected sub-frames. This was a major challenge in the 3GPP Rel-10 and earlier LTE systems, because only one CSI feedback process was allowed. There were no good mechanisms for a receiver to perform accurate CSI measurement over protected sub-frames, especially when different combinations of muting patterns for neighboring interfering cells needed to be considered. However, in the 3GPP Rel-12 LTE-A systems, to support the use of coordinated multi-point (CoMP) transmission, a set of zero-power CSI reference symbols (CSI-RS) is standardized. The receiver can use the zero-power CSI-RS to perform accurate CSI measurement when certain neighboring interfering cells are muted. Several CSI feedback processes can be initiated to report different channel qualities when different muting patterns for neighboring interfering cells are applied. Details about the configuration of

Table 2 Average ABS ratio configured by micro cells

Number of VUEs and VPL	Backhaul schemes			
	IRC	MRC	30% ABS	37% ABS
Random VUEs, 15 dB VPL	0.0920	0.0813	0.0740	0.0663
25 VUEs, 15 dB VPL	0.0884	0.0848	0.0671	0.0697
Random VUEs, 30 dB VPL	0.0250	0.0250	0.0250	0.0250
25 VUEs, 30 dB VPL	0.0250	0.0250	0.0250	0.0250

zero-power CSI-RS and the feedback mechanism can be found in ([62] Ch. 15). Therefore, no new feedback mechanisms need to be standardized to perform the scheduling restriction algorithm considered in this study. We need to emphasize that from Equation 9 and Equation 12, we see that only the average throughput is required to apply the scheduling restrictions. Therefore, a receiver only needs to feed back the CSI measurement or the estimated average throughput for different muting patterns of neighboring interfering cells once per every several sub-frames, e.g., one or several ABS cycles. Therefore, only limited feedback overhead is expected. Hence, the tools offered by the current LTE-A systems can adequately support using ABSs together with the scheduling restrictions considered in our study.

As discussed in Section 5, for using multi-antenna receivers for MNs to enhance the backhaul links, two schemes, i.e., the MRC and IRC receivers, are considered in this study. Because these are schemes applied at the receiver ends, no CSI at the transmitters (CSIT) is required. Therefore, there are no impacts on the network side. For the MRC receivers, it is only necessary to estimate the desired channel coefficient for each of the antennas of the receiver. In our study, we assumed perfect channel knowledge, both for the desired and interference signals. In practical LTE-A systems, the channel estimation is usually achieved through the cell specific reference signal (CRS), which is orthogonal between neighboring cells ([62] Ch. 10). Moreover, joint channel estimation and signal detection can be used to achieve fairly good performance, e.g., using linear-minimum-mean-square-error (LMMSE) estimation [63,64]. The complexity of the channel estimation algorithm varies. If we consider N_c as the number of subcarriers in the OFDMA system, the LMMSE channel estimator has a complexity of $O(N_c^3)$ [64], but low-complexity channel estimation algorithms with comparable performance to the LMMSE algorithm can reduce the complexity to $O(N_c \log N_c)$ [64]. Depending on the carrier frequency, the density of CRS in the current LTE-A system supports accurate channel estimation for a user velocity up to 500 km/h ([16] Ch. 1). Therefore, for the speed of the MNs considered in our study, the accuracy of channel estimation is not a major concern.

However, when using IRC receivers, not only the desired channel coefficients at each of the receiving antennas need to be estimated but also a knowledge of the interference channels at the receiver is required. In addition to the complexity of channel estimation, the additional complexity of $O(N_c^3)$ is introduced by the IRC receivers because of the estimation and inversion of the channel covariance matrix for the interference signals [65]. In practice, as discussed above, the desired channel coefficients can be easily estimated. Various methods can be applied to obtain

fairly good estimation of the channel information of the interference signals. To understand the feasibility and performance in using IRC receivers in LTE-A systems, in [66,67] simulations were performed. The results in [66,67] show that by either using data signal-based interference estimation or demodulation reference signal (DMRS)-based interference estimation, the channel of the interfering signaling can be well estimated to enable the IRC receivers to be used in the LTE-A system, and significant cell-edge throughput improvement is observed in the use of IRC receivers. Therefore, the current LTE-A systems have good support for the multi-antenna receivers considered in our study.

Certain changes are required on the current LTE-A system to support the use of ABSs for the micro cells to protect the access links of the MNs. As discussed in Section 6, the micro cells adjust the number of ABSs based on the feedback of MNs. The feedback of the MNs cannot be directly made available at the micro cells, because there are no direct connections between the MNs and the micro cells. Therefore, it is more likely that the network needs to collect the feedback from the MNs, and then configure the ABS patterns at the micro cells accordingly. As discussed in Section 4.1, because the update of ABSs usually occurs in minutes, a slow feedback link between each of the MNs and the network is sufficient to convey this information.

8.2 Limitations in the current LTE-A systems

As mentioned in Section 3, in this study, we align most of our assumptions with the current FDD LTE-A systems. To perform link adaptations at the BSs, the UEs need to feed back their channel quality indication (CQI) to the BSs.^k In an FDD LTE-A system, a UE can be set up to feed back CQI every 2 ms. However, because of system load, scheduling and frame structures in the current FDD LTE-A systems, a feedback delay between 4 and 10 ms can be expected ([62] Ch. 11, 13). The feedback delay is not a significant problem for low speed UEs but may cause problems at vehicular speeds. In [68], it was argued that the sensitivity of the coding and modulation schemes can be adjusted, and an upper limit of 0.15 for the normalized mean square error of the CQI can be tolerated. In [68], it was further demonstrated that the use of a Kalman-filter-based channel predictor could improve the reliability of the CQI feedback. From Figure 3, we see that most of the UEs, as well as the backhaul links of the MNs, have a fairly good SNR,^l and therefore, according to the study in [68], fairly good performance of link adaptation can be expected at the velocity of the MNs considered in this study, i.e., 50 km/h. However, this might be a problem for higher speeds. On the one hand, in the future 5G systems, if the length of the sub-frames can be shortened, and the feedback delays can be further reduced, the channel predictors should be able to

support much higher speed. On the other hand, because MNs are less constrained by power, antenna element size, and transceiver complexity, it is less costly to integrate more sophisticated multi-antenna schemes and advanced signal processing algorithms into MNs compared with regular UEs. As demonstrated in [41,42], by using the so-called predictor antennas on top of a vehicle, reliable CSIT can be obtained at the transmitter side to support various closed-loop MIMO schemes. This is another big advantage in using MNs to serve VUE devices.

Our results in Section 7 show that the design of the current LTE-A system limits the benefits of using MNs. First, as discussed in Section 7.1, the same coding and modulation schemes are required for the PRBs allocated to the same user at one sub-frame. This limits the gains of frequency adaptive transmission and has a greater impact on the backhaul links of MNs than regular UEs, because the number of PRBs allocated to the backhaul links of an MN is proportional to the number of VUEs it serves, i.e., per-PRB-based link adaptation would be beneficial [69]. Second, even if the SINR at the backhaul links are improved by using various ICIC schemes (see Figure 6), the throughput does not necessarily increase. Certain macro sub-frames need to be muted when using ABS to mitigate interference, therefore improving the SINR statistics, but the total throughput suffers from the muting of the macro sub-frames. Furthermore, in medium SINR regions, the throughput saturates because of the coding and modulation schemes used in the LTE-A system. Currently, only up to 64-QAM is used as the highest modulation order. In the current LTE-A systems, if a single antenna is used at the BS, the throughput saturates at 30 dB SINR ([70]

Ch. 5). In Figure 6, we observe that by using MRC, around 30% of the PRBs of the backhaul links of the MNs have more than 30 dB SINR, and if IRC is used over 80% of the PRBs of the backhaul links of the MNs have more than 30 dB SINR. Therefore, if higher order modulation can be used, e.g., 256-QAM ([70] Ch. 5), the throughput of the backhaul links can be further improved. To demonstrate these two points, in Figure 23, we plot the achievable throughput for the VUEs when the rate at backhaul links is calculated on a per PRB basis using the Shannon capacity formula at VPL 15 dB, and MRC receivers are used at the backhaul links of MNs. Compared with when applying LTE-A scheduling restrictions, we observe that the improvement is obvious. Thus, the benefits of MNs can be better exploited in future broadband wireless networks with further enhanced capabilities.

8.3 Further works

Another concern in deploying MNs is that unwanted UEs might be attached to the nearby MNs. This is not a major problem when the public transportation vehicle is moving at a regular speed, because the handover criteria are not easily satisfied unless a UE is moving parallel to the public transportation vehicle at similar speed. However, in situations in which public transportation vehicles move slowly or stop, e.g., in traffic congestion during rush hours or picking up passengers at bus stops, this may be a big problem. Therefore, solutions that optimize the user admission and handover criteria are also of great importance in future studies using MNs. Similar ideas from the research of femto cells can be borrowed [71,72], e.g., an MN only admits the users that have similar mobility characteristic

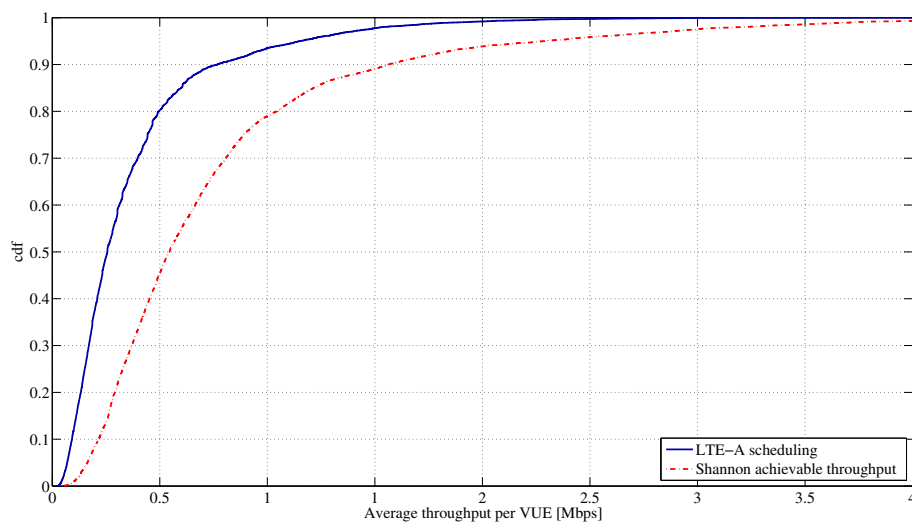


Figure 23 The cdf of VUE Shannon capacity based throughput on a per PRB basis, uniformly distributed VUEs, VPL at 15dB. The solid blue line is the cdf of VUE throughput when we considered the LTE-A scheduling constraints. The dash-dot red line is the cdf of VUE achievable throughput calculated on a per PRB basis by using the Shannon capacity.

to itself, or it sets a relatively higher handover margin to limit its coverage area inside the vehicle as much as possible. In [12], we provided a framework to optimize the handover parameters for the use of MRN. Nevertheless, this issue requires more thorough research.

In this study, we consider the MNs are moving at a constant speed and only serve the users inside the vehicles. However, in scenarios in which MNs have relatively low mobility and high density, their use can be extended in several different ways. For example, during traffic congestion in rush hours, some public transportation vehicles may become stuck in bad coverage areas for quite a long time. Therefore, we may consider enabling multi-hop communication between the backhaul links of MNs. In this way, the capacity of the mobile network can be better distributed across the service area of one or several BSs, and the VUE experience may be significantly improved. Certainly, there are several challenges to support multi-hop communication between the MNs. The future 5G system offers a good opportunity for this, especially when new low latency and high capacity air interfaces are developed. Moreover, this is very similar to a typical MANET scenario, and therefore power control and interference management schemes developed for MANET and D2D communication can be applied to facilitate the multi-hop communication. Furthermore, in such scenarios, we may also consider using the MNs to serve the UEs that are outside the public transportation vehicles. Hence, more users can benefit from the deployment of MNs.

Nowadays, there are commercially available solutions that use a cellular network as a backhaul and use WiFi as the access technology to provide Internet services to VUEs [7,73]. The benefits and limitations of using WiFi to serve VUEs are briefly discussed in [7]. As this solution is totally based on using existing network elements, it can be deployed very fast. Moreover, advantages, such as eliminating the VPL can also be realized. However, as WiFi-based solutions are usually offered by third party companies, rather than mobile operators, and the limitations are also very obvious. As pointed out in Section 3, if a WiFi hot spot is treated simply as a regular UE that has a high data-rate demand, it is not certain that the fairness between VUEs and other UEs served by the same BS can be maintained. Moreover, because WiFi is operating in the open industrial, scientific and medical (ISM) radio bands, the interference management and channel selections for the WiFi access link are achieved in a distributed self-organized manner [74,75]. Therefore, if we further exploit the potential of using WiFi as the access technology to serve VUEs, better interference management schemes need to be developed for the WiFi access links, especially in a densely deployed urban scenario where WiFi hot spots are randomly and densely deployed.

Potentially a tightly operator controlled WiFi solution is required in this case.

As pointed out in [76,77], channel modeling is very important in the study of 5G communication systems. The EU 5G project METIS is also developing new channel models that can better serve the needs of 5G system simulations, e.g., the METIS channel models are expected to provide good spatial consistency, which is not well supported in the currently available channel models. Accurate spatial consistency is needed to evaluate the performance of spatial techniques, e.g., multi-user MIMO, where the performance may be exaggerated because of non-independent fading. Before the METIS channel models are finished, the ITU-R Uma and Umi models are suggested by METIS [14] to model small scale fading. We expect limited impacts on the results presented in this study from the new channel models that are under development in METIS. This is because the schemes that we consider in this study do not rely on the use of spatial techniques. Moreover, because of the size of public transportation vehicles, low correlation between antenna elements can be achieved. Around 18 cm distance between antenna elements is needed at 800 MHz to achieve low enough correlations, and cross polarized placements can be used to further lower the correlation between two antenna elements. A single antenna is considered at each BS sector, and adequate separation is assumed between the antennas of each of the sectors. Therefore, as long as enough separation between the receiver antennas can be achieved, we can safely assume independent fading between each of the links. Nevertheless, when extending the study of MNs in future research, especially when various spatial MIMO techniques are considered in both macro and micro cells, using the newly developed METIS channel models or other channel models that provide support for good spatial consistency, should be considered.

The cost of deploying MNs on public transportation vehicles can be recouped by bringing in more business opportunities for both operators and service providers. For example, the MNs can push personalized information to travelers, e.g., weather or traffic information, both to improve customer loyalty and potentially generate more revenue for the operators and service providers. Using MNs can also bring several benefits for the network side and is an indispensable enabler of content caching at the BSs and context aware communication [78-80]. For example, at different times of the day, the MNs can cache commonly accessed content according to the previous habits of the commuters. This not only reduces the latency but also lessens the load on the macro cells.

9 Conclusions

In general, MNs can improve the throughput for the VUEs without significantly affecting the performance of

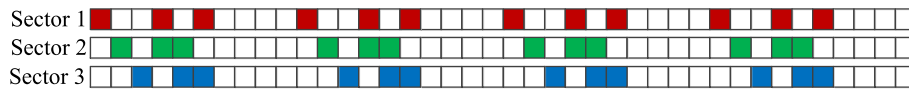


Figure 24 Frames with ABS patterns for three macro sectors in the case of 30% ABS. Colored subframes are ABSs.

outdoor UEs. From the results in Section 7, we see that the backhaul links are the bottlenecks to further improving the performance of the MNs. Compared with noise-limited scenarios and scenarios with limited interference [7,11,12,28], in a densely deployed urban scenario, interference is the biggest factor affecting the performance of MNs, which is why the IRC scheme for the backhaul links of MNs gives the most gain. Compared with regular UEs, public transportation vehicles are less constrained by power, antenna size, and transceiver complexity. Even though, in this study, we only considered using multi-antennas at the receiver end, more advanced signal processing and multi-antenna schemes, e.g., using predictor antennas [41,42], can be realized for MNs to further improve their performance. Moreover, when lacking the CSI from the interferers, ABSs can be combined with the MRC scheme. In this way, potentially fewer ABSs can be used, and better performance can be expected for both the outdoor UEs and the VUEs. Nevertheless, the use of MNs is a good solution in the next-generation system for improving the user experience on VUE.

9.1 Table of notations

A table of notations is provided in Table 3.

Endnotes

^a5GNOW stands for 5th Generation Non-Orthogonal Waveforms for Asynchronous Signaling.

^bVPL is the outdoor-to-indoor signal attenuation caused when the signal penetrates through the vehicle.

^cIn order to have a concrete and practical description of the challenges in various scenarios faced by future mobile communication system, 12 different test cases have been selected by METIS.

^dCoordination between several macro and micro cells are needed in order to configure ABSs patterns.

^eA dominant eigenvector is the eigenvector corresponding to the eigenvalue of the biggest absolute value.

^fThe initial value can be either selected based on long-term observation or simply set to the lowest value.

^gSoftware implementation of the METIS pathloss and shadowing is available at <https://www.metis2020.com/documents/simulations/>, last accessed on 2015-02-01.

^hSoftware implementation of the ITU-R channel model is available at <https://www.itu.int/oth/R0A06000022/en>, last accessed on 2015-02-01.

ⁱIn the current LTE-A system, all the PRBs that are allocated to the same UE are required to use the same coding and modulation scheme ([16] Ch. 9 and 10).

^jUnlike CRS, DMRS is UE specific and standardized for more flexible MIMO operations in LTE-A systems ([62] Ch. 10).

^kLink adaptation only requires the amplitude information of the channel, and no feedback of phase information is needed.

^lThe channel prediction is based on pilot signals from each cell, which is usually orthogonal to each other among neighboring cells. The pilot symbols may be interfered by data symbols, but the system can boost the power of the pilot symbols for better channel estimation and prediction ([62] Ch. 11, 13).

Appendix

The detailed ABS patterns used for the macro BS sectors are plotted on Figures 24 and 25. Please note that these are only representative patterns considered in the simulations. In a practical system, some restrictions may apply to the positions of ABSs [22]. We remark that the choice of 30% ABSs (12 ABSs out of 40 subframes) is based on the SINR distribution when no ICIC scheme is considered (see Figure 6) and the constraint that the number of ABSs needs to be an integer. For the 37.5% ABSs case, compared to the 30% ABSs case, 3 more ABSs are added to have stronger protection of both type 2 and type 3 UEs.

Regarding the ABS configurations for the micro cells, we initialize the first subframe as ABS for all the micro cells. Then, we follow Algorithm 1. If any of the MNs report insufficient number of ABSs, one more arbitrary subframe is added as ABS for more protection. We iterate this process until the average throughput of the access link of the

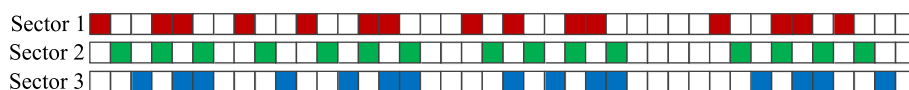


Figure 25 Frames with ABS patterns for three macro sectors in the case of 37.5% ABS. Colored subframes are ABSs.

Table 3 Table of notations

Symbol	Meaning
$b(l, m, u)$	The scheduling decision for the u th user in m th PRB in the l th subframe
$b_p(n)$	Total number of PRBs scheduled for device n over \mathcal{R}_p
$b_{np}(n)$	Total number of PRBs scheduled for device n over \mathcal{R}_{np}
$d(n)$	A function that measures channel quality difference for the n th device over the protected and non-protected PRBs
i_v	The number of active VUEs on the v th MN
j	The index of an interferer
k	The time index of received signal
l	The index of a subframe
m	The index of a PRB in a given subframe
n	The index of an arbitrary device, i.e., either a UE or an MN, connecting to a macro cell
$n^*(l, m)$	The device is selected to be scheduled at the m th PRB in the l th subframe in the macro cell
p	The number of antennas equipped at the backhaul link of an MN
q_{n_1}	An arbitrary device served by macro BS sector 1
$r(l, m, u)$	The throughput of the u th macro UE at the m th PRB in the l th subframe
$r_{0j}(v)$	The throughput of the access link of the v th MN when the j th subframe in the micro cells is configured as ABS
$r_{1i}(v)$	Throughput of the access link of the v th MN when the i th subframe in the micro cells is not configured as ABS
$r_p(n)$	The average rate of device n over \mathcal{R}_p
$r_{np}(n)$	The average rate of device n over \mathcal{R}_{np}
$s(n)$	The average throughput of device n , which can be either a macro UE or the backhaul link of an MN
$s(u)$	The average throughput of the u th macro UE
$s(v)$	The average throughput of the backhaul link of the v th MN
u	The index of a macro UE
$u^*(l, m)$	The macro UE that is selected to be scheduled at the m th PRB in the l th subframe
x_k	The desired signal transmitted at time k
$x_{j,k}$	The interfering signal from the j th interferer at time k
n_1	The index of a device served by macro BS sector 1
v	The index of an MN
B_p	The size of \mathcal{R}_p
B_{np}	The size of \mathcal{R}_{np}
$G(v)$	$G(v) = N \frac{v}{(1+v)}$ for $v \geq 0$, a function defined to facilitate the solution of problem (7)
K	A parameter used in the solution of (11), where $K \in \{0, 1, \dots, N-1\}$ and $G(d(K+1)) \leq K \leq G(d(K))$
L	The number of total subframes in which the average throughput of a device in the macro cell is calculated
M	The total number of PRBs in each subframe
N	The total number of devices, i.e., $N = N_u + N_m$, connect to a macro cell
N_1	The number of devices served by macro BS sector 1

Table 3 Table of notations (Continued)

N_c	The number of subcarriers in an OFDMA system
N_L	The number of interferers experienced at the backhaul link of an MN
N_m	The number of MNs in a macro cell
N_u	The number of macro UEs in a macro cell
N_{sf}	The number of total subframes that average throughput target of the backhaul link of the MNs are calculated in the micro cells
$\bar{R}(v)$	The average throughput target of the backhaul link of the v th MN during N_{sf} subframes
α	A parameter used in the solution of (11), where $\alpha = \lambda_p - K$
γ_k	The instantaneous output SINR at the MN backhaul receiver at time k
ε	An averaging constant that is required in updating the average throughput of a given device
λ_p	A parameter used in the solution of (11), where $\lambda_p = \max(G(d(K+1)), K)$
λ_{np}	A parameter used in the solution of (11), where $\lambda_{np} = N - \lambda_p$
σ_n^2	The noise power at each antenna
$\mu(l, u)$	The average throughput of user u
\mathcal{I}_i	$\mathcal{I}_i \in \{0, 1\}$, $i = 1, 2, 3 \dots N_{sf}$ indicate the status of the ABSs at the micro cells
\mathcal{M}	The sets denotes all the macro UEs in a cell
\mathcal{R}_p	The set of protected PRBs in a macro cell
\mathcal{R}_{np}	The set of non-protected PRBs in a macro cell
\mathcal{S}_1	The set of users only scheduled in \mathcal{R}_p
\mathcal{S}_2	The set of users only scheduled in \mathcal{R}_{np}
\mathcal{S}_3	The set of users can be scheduled both in \mathcal{R}_p and \mathcal{R}_{np}
\mathcal{U}	To denote uniform distribution
\mathcal{V}	The sets denotes all the MNs in a cell
\mathbf{h}_k	The channel vector of the desired signals at each receiver antenna of an MN at time k
$\mathbf{h}_{j,k}$	The channel vector of the j th interfering signal observed at each receiver antenna of an MN at time k
\mathbf{n}_k	The vector denotes the thermal noise at each receiver antenna of an MN at time k
\mathbf{w}_k	The vector that contains the weight applied at each receiver antenna of an MN at time k
\mathbf{y}_k	The vector that contains the received signal at each receiver antenna of an MN at time k
\mathbf{z}_k	The combined signal at the output of an MN backhaul receiver at time k
\mathbf{R}	The noise covariance matrix of the receiver antennas of an MN
$I_{p \times p}$	The identity matrix of size p
$(\cdot)^H$	To denote the complex conjugate transpose of a matrix
$\text{ElG}_{\max}(\cdot)$	To denote the dominant eigenvector of a matrix

worst MN in that area is satisfied. The ABS configurations is reset at the beginning of each drop.

Competing interests

The authors declare that they have no competing interests.

Acknowledgments

Part of this work has been performed in the framework of the FP7 project ICT-317669 METIS, which is partly funded by the European Union. The authors would like to acknowledge the contributions of their colleagues in METIS, although the views expressed are those of the authors and do not necessarily represent the project. This work is also supported by the Swedish Research Council VR under the project 621-2009- 4555 Dynamic Multipoint Wireless Transmission, and in part by United States National Science Foundation grant CNS-1406968.

Author details

¹Department of Signals and Systems, Chalmers University of Technology, EDIT-huset, Hörsalsvägen 9-11 Gothenburg, SE-41296, Sweden. ²Electrical and Computer Engineering, Florida International University, 10555 W Flagler Street, EC 3142, Miami, FL 33174-1630, USA.

Received: 31 October 2014 Accepted: 10 March 2015

Published online: 18 April 2015

References

1. Hwang, B Song, SS Soliman, A holistic view on hyper-dense heterogeneous and small cell networks. *IEEE Commun. Mag.* **51**, 20–27 (2013). doi:10.1109/MCOM.2013.6525591
2. IS Gaspar, G Wunder, 5G Cellular communications scenarios and system requirements. Technical report. [Online, last accessed 2014-10-01] <https://www.5gnow.eu>
3. JG Andrews, S Buzzi, W Choi, S Hanly, A Lozano, ACK Soong, JC Zhang, What will 5G be? *IEEE J. Sel. Areas Commun., Special Issue on 5G Commun. Syst.* **32**(6), 1065–1081 (2014). doi:10.1109/JSAC.2014.2328098
4. P Popovski, V Braun, H-P Mayer, P Fertl, DG-S Zhe Ren, E Ström, T Svensson, H Taoka, P Agyapong, A Benjebbour, G Zimmermann, J Meinilä, J Ylitalo, T Jämsä, P Kyösti, K Dimou, M Fallgren, Y Selen, B Timus, H Tullberg, M Schellmann, Y Wu, M Schubert, DH Kang, JI Markendahl, C Beckman, M Uusitalo, O Yilmaz, C Wijting, Z Li, et al., ICT-317669-METIS/ D1.1 Scenarios, requirements and KPIs for 5G mobile and wireless system. Technical report. [Online, last accessed 2014-10-01] <https://www.metis2020.com>
5. 3GPP TR 36.836, Technical specification group radio access network: mobile relay for evolved universal terrestrial radio access (E-UTRA). Technical report. [Online, last accessed 2014-10-01] <http://www.3gpp.org>
6. W Phan, K Horneman, L Yu, J Vihriälä, in *Proc. IEEE Veh. Netw. Conf. (VNC)*. Providing enhanced cellular coverage in public transportation with smart relay systems (Jersey City, 2010)
7. Y Sui, J Vihriälä, A Papadogiannis, M Sternad, T Svensson, Moving cells: a promising solution to boost performance for vehicular users. *IEEE Commun. Mag.* **51**, 62–68 (2013). doi:10.1109/MCOM.2013.6525596
8. D Aronsson, H Bonneville, B Fan, M Färber, J Gora, M Khanfouci, G Liebl, TM de Moraes, A Nicolov, S Redana, A Saadani, E Seidel, M Sternad, T Svensson, J Vihriälä, D3.4 relay configurations. Technical report (Artist4G deliverable, Jul. 2011). [Online, last accessed 2014-10-01] <https://ict-artist4g.eu/projet/deliverables>
9. E Tanghe, W Joseph, L Verloock, L Martens, Evaluation of vehicle penetration loss at wireless communication frequencies. *IEEE Trans. Veh. Technol.* **57**(4), 2036–2041 (2008). doi:10.1109/TVT.2007.912164
10. Huawei Technologies: Whitepaper on spectrum. Technical report (Feb. 2013). [Online, last accessed 2014-10-01] <http://www.huawei.com>
11. Y Sui, A Papadogiannis, T Svensson, in *Proc. IEEE Veh. Tech. Conf. (VTC)*. The potential of moving relays - a performance analysis (Yokohama, 2012)
12. Y Sui, Z Ren, W Sun, T Svensson, P Fertl, in *Proc. IEEE Int. Conf. on Connected Veh. and Expo (ICCVE)*. Performance study of fixed and moving relays for vehicular users with multi-cell handover under co-channel interference (Las Vegas, 2013)
13. A Damjanovic, J Montojo, Y Wei, T Ji, T Luo, M Vajapeyam, T Yoo, O Song, D Malladi, A survey on 3GPP heterogeneous networks. *IEEE Trans. Wireless Commun.* **18**(3), 10–21 (2011). doi:10.1109/MWC.2011.5876496
14. P Agyapong, V Braun, M Fallgren, A Gouraud, M Hessler, S Jeux, A Klein, J Lianghai, D Martin-Sacristan, M Maternia, M Moisis, JF Monserrat, K Pawlak, H Tullberg, A Weber, ICT-317669-METIS/D6.1 Simulation guidelines. Technical report (2013). [Online, last accessed 2014-10-01] <https://www.metis2020.com>
15. HS Dhillon, RK Ganti, F Baccelli, JG Andrews, Modeling and analysis of K-tier downlink heterogeneous cellular networks. *IEEE J. Sel. Areas Commun.* **30**(3), 550–560 (2012). doi:10.1109/JSAC.2012.120405
16. S Sesia, I Toufik, M Baker, *LTE - The UMTS Long Term Evolution: From Theory to Practice*, 2nd edition. (John Wiley & Sons Ltd, West Sussex, UK, 2011)
17. P Ökvist, A Simonsson, in *Proc. IEEE Veh. Tech. Conf. (VTC)*. LTE HetNet Trial - Range expansion including micro/pico indoor coverage survey (Quebec City, 2012)
18. M Shirakabe, A Morimoto, N Miki, in *Proc. Int. Symp. on Wireless Commun. Syst. (ISWCS)*. Performance evaluation of inter-cell interference coordination and cell range expansion in heterogeneous networks for LTE-Advanced downlink (Aachen, 2011)
19. P Bhat, S Nagata, L Campoy, I Berberana, T Derham, G Liu, X Shen, P Zong, J Yang, LTE-Advanced: an operator perspective. *IEEE Commun. Mag.* **50**, 104–114 (2012). doi:10.1109/MCOM.2012.6146489
20. TQS Quek, G de la Roche, I Guvenc, M Kountouris (eds.), *Small Cell Networks: Deployment, PHY Techniques, and Resource Management* (Cambridge University Press, Cambridge, UK, 2013)
21. A Anpalagan, M Bennis, R Vannithamby (eds.), *Time and Frequency Domain e-ICIC with Carrier Aggregation in HetNets* (Cambridge University Press, Cambridge, UK, 2014)
22. ST-Ericsson Ericsson, R1-105335: Details of almost blank subframes. Technical report (Oct. 2010). [Online, last accessed 2014-10-01] <http://www.3gpp.org>
23. S Deb, P Monogioudis, J Miernik, JP Seymour, Algorithms for enhanced inter-cell interference coordination (eICIC) in LTE HetNets. *IEEE/ACM Trans. Netw.* **22**, 137–150 (2014). doi:10.1109/TNET.2013.2246820
24. NTT DOCOMO, R1-103264: Performance of eICIC with control channel coverage limitation. Technical report (May 2010). [Online, last accessed 2014-10-01] <http://www.3gpp.org>
25. 3GPP TR 36.866, Study on network-assisted interference cancellation and suppression (NAICS) for LTE. Technical report (2014). [Online, last accessed 2014-10-01] <http://www.3gpp.org>
26. IEEE 802.16 Broadband Wireless Access Working Group: IEEE C802.16j-07/087r2 mobile relay station operation. Technical report (2007). [Online, last accessed 2014-10-01] <http://www.ieee802.org/16/>
27. P Mach, Z Becvar, in *Proc. Int. Conf. on Netw. (ICN)*. Path selection in WiMAX networks with mobile relay stations (Toronto, 2011)
28. Y Sui, A Papadogiannis, W Yang, T Svensson, in *Proc. IEEE Global Commun. Conf. (GLOBECOM) Workshops*. Performance comparison of fixed and moving relays under co-channel interference (Anaheim, 2012)
29. Y Sui, A Papadogiannis, W Yang, T Svensson, in *Proc. IEEE Veh. Tech. Conf. (VTC)*. The energy efficiency potential of moving and fixed relays for vehicular users (Las Vegas, 2013)
30. I Chlamtaca, M Contib, JJ-N Liuc, Mobile ad hoc networking: imperatives and challenges. *Ad Hoc Netw.* **1**, 13–64 (2003). doi:10.1016/S1570-8705(03)00013-1
31. MN Tehrani, M Uysal, H Yanikomeroğlu, Device-to-device communication in 5G cellular networks: challenges, solutions, and future directions. *IEEE Commun. Mag.* **52**, 86–92 (2014). doi:10.1109/MCOM.2014.6815897
32. L Lei, Z Zhong, C Lin, X Shen, Operator controlled device-to-device communications in LTE-advanced networks. *IEEE Trans. Wireless Commun.* **19**, 96–104 (2012). doi:10.1109/MWC.2012.6231164
33. X Lin, JG Andrews, A Ghosh, R Ratasuk, An overview of 3GPP device-to-device proximity services. *IEEE Commun. Mag.*, 40–48 (2014). doi:10.1109/MCOM.2014.6807945
34. Z Ren, S Stanczak, P Fertl, F Penna, in *Proc. IEEE Int. Conf. on Commun. (ICC)*. Energy-aware activation of nomadic relays for performance enhancement in cellular networks (Sydney, 2014). doi:10.1109/ICC.2014.6883765
35. H Min, J Lee, S Park, D Hong, Capacity enhancement using an interference limited area for device-to-device uplink underlying cellular networks. *IEEE Trans. Wireless Commun.* **10**, 3995–4000 (2011). doi:10.1109/TWC.2011.100611.101684
36. G Fodor, E Dahlman, G Mildh, S Parkvall, N Reider, G Miklós, Z Turányi, Design aspects of network assisted device-to-device communications.

- IEEE Commun. Mag. **50**, 170–177 (2012). doi:10.1109/MCOM.2012.6163598
37. A Papadogiannis, Y Sui, T Svensson, in *Proc. IEEE Veh. Tech. Conf. (VTC)*. The potential of a hybrid fixed/user relay architecture—a performance analysis (Québec City, 2012). doi:10.1109/VTCFall.2012.6399279
 38. NL Pradhan, T Saadawi, Power control algorithms for mobile ad hoc networks. *J. Adv. Res.* **2**, 199–206 (2011). doi:10.1016/j.jare.2011.04.009
 39. P Janis, V Koivunen, C Ribeiro, J Korhonen, K Doppler, K Hug, in *Proc. IEEE Veh. Tech. Conf. (VTC)*. Interference-aware resource allocation for device-to-device radio underlying cellular networks (Barcelona, 2009). doi:10.1109/VETECS.2009.5073611
 40. C-H Yu, K Doppler, CB Ribeiro, O Tirkkonen, Resource sharing optimization for device-to-device communication underlying cellular networks. *IEEE Trans. Wireless Commun.* **10**, 2752–2763 (2011). doi:10.1109/TWC.2011.060811.102120
 41. M Sternad, M Grieger, R Apelfrojd, T Svensson, D Aronsson, AB Martinez, in *Proc. IEEE Wireless Commun. and Netw. Conf. (WCNC) Workshop*. Using 'predictor antennas' for long-range prediction of fast fading for moving relays (Paris, 2012)
 42. D-T Phan-Huy, M Sternad, T Svensson, in *Proc. IEEE Int. Conf. on Connected Veh. and Expo (ICCVE)*. Adaptive large MISO downlink with predictor antennas array for very fast moving vehicles (Las Vegas, 2013)
 43. W Li, C Zhang, X Duan, S Jia, Y Liu, L Zhang, in *Proc. IEEE Veh. Tech. Conf. (VTC)*. Performance evaluation and analysis on group mobility of mobile relay for LTE-Advanced system (Quebec City, 2012)
 44. P Popovski, V Braun, G Mange, P Fertl, D Gozalvez-Serrano, N Bayer, H Droste, A Roos, G Zimmermann, M Fallgren, A Höglund, H Tullberg, S Jeux, Ö Bulakci, J Eichinger, Z Li, P Marsch, MB Krystian Pawlak, JF Monserrat, ICT-317669-METIS/D6.2 Initial report on horizontal topics, first results and 5G system concept. Technical report (2014). [Online, last accessed 2014-10-01] <https://www.metis2020.com>
 45. P Popovski, G Mange, P Fertl, D Gozalvez-Serrano, H Droste, N Bayer, A Roos, T Rosowski, G Zimmermann, P Agyapong, M Fallgren, N He, A Höglund, J Söder, H Tullberg, S Jeux, Ö Bulakci, J Eichinger, M Schellmann, J Lianghai, A Rauch, A Klein, M Stamatelatos, Z Li, M Moision, M Maternia, E Lähetkangas, K Pawlak, JF Monserrat, D Martin-Sacristán, ICT-317669-METIS/D6.3 Intermediate system evaluation results. Technical report (2014). [Online, last accessed 2014-10-01] <https://www.metis2020.com>
 46. F Kelly, A Maulloo, D Tan, Rate control for communication networks: shadow prices, proportional fairness and stability. *Oper. Res. Soc.* **49**, 237–252 (1998). doi:10.1057/palgrave.jors.2600523
 47. MR Jeong, N Miki, A simple scheduling restriction scheme for interference coordinated networks. *IEICE Trans. Commun.* **E96-B(6)**, 1306–1317 (2013)
 48. G Caire, R Muller, R Knopp, Hard fairness versus proportional fairness in wireless communications: the single-cell case. *IEEE Trans. Inf. Theory.* **53**, 1366–1385 (2007). doi:10.1109/TIT.2007.892790
 49. P Mogensen, W Na, IZ Kovacs, F Frederiksen, A Pokhariyal, KI Pedersen, T Kolding, K Hugi, M Kuusela, in *Proc. IEEE Veh. Tech. Conf. (VTC)*. LTE capacity compared to the Shannon bound (Dublin, 2007). doi:10.1109/VETECS.2007.260
 50. G Piro, LA Grieco, G Boggia, F Capozzi, P Camarda, Simulating LTE cellular systems: an open source framework. *IEEE Trans. Veh. Technol.* **60**, 498–513 (2011). doi:10.1109/TVT.2010.2091660
 51. M Cierny, H Wang, RR Wichman, Z Ding, C Wijting, On number of almost blank subframes in heterogeneous cellular networks. *IEEE Trans. Wireless Commun.* **12**, 5061–5073 (2013). doi:10.1109/TWC.2013.090513.121756
 52. D Lopez-Perez, X Chu, in *Proc. Int. Conf. on Comput. Commun. and Netw (ICCCN)*. Inter-cell interference coordination for expanded region picocells in heterogeneous networks (Maui, 2011)
 53. Y Peng, F Qin, in *Proc. IEEE Int. Conf. on Commun. (ICC)*. Exploring Het-Net in LTE-Advanced system, interference mitigation and performance improvement in macro-pico scenario (Kyoto, 2011)
 54. AF Molisch, *Wireless Communications*, 2nd edition. (John Wiley & Sons Ltd, West Sussex, UK, 2010)
 55. DG Brennan, Linear diversity combining techniques. *Proc. IEEE.* **47**, 1075–1102 (1959). doi:10.1109/JPROC.2002.808163
 56. J Zhang, J Olivier, A Sayeed, BV Veen, in *Proc. IEEE Veh. Tech. Conf. (VTC)*. Low complexity MIMO receiver via maximum SINR interference cancellation (Birmingham, 2002)
 57. P Marsch, GP Fettweis (eds.), *Coordinated Multi-Point in Mobile Communications From Theory to Practice* (Cambridge University Press, Cambridge, UK, 2011)
 58. A Schrijver, *Theory of Linear and Integer Programming*. (John Wiley & Sons, West Sussex, England, 1998)
 59. M Simsek, M Bennis, A Czyliwki, in *Proc. IEEE Global Commun. Conf. (GLOBECOM)*. Dynamic inter-cell interference coordination in HetNets: a reinforcement learning approach (Anaheim, 2012)
 60. International Telecommunication Union, Guidelines for evaluation of radio interface technologies for IMT-Advanced. Technical report (2009). [Online, last accessed 2014-10-01] <http://www.itu.int/>
 61. P Gupta, V Agarwal, M Varshney, *Design and Analysis of Algorithms*, Second Edition. (PHI Learning Pvt. Ltd., New Delhi, India, 2012)
 62. E Dahlman, S Parkvall, J Skold, *4G: LTE/LTE-Advanced for Mobile Broadband*, Second Edition. Academic Press, Waltham, MA, USA, 2014)
 63. H Schoeneich, PA Hoehner, Iterative pilot-layer aided channel estimation with emphasis on interleave-division multiple access systems. *EURASIP J. Appl. Signal Process.* **2006**, 1–15 (2006). doi:10.1155/ASP/2006/81729
 64. N Geng, X Yuan, L Ping, Dual-diagonal LMMSE channel estimation for OFDM systems. *IEEE Trans. Signal Process.* **60**, 4734–4746 (2012). doi:10.1109/TSP.2012.2202112
 65. Z YAN, G He, J Ma, An enhanced IRC algorithm for LTE downlink receiver in multi-cell environment. *Chin. J. Electron.* **23(2)**, 377–381 (2014)
 66. Y Ohwatari, N Miki, T Asai, T Abe, H Taoka, in *Proc. IEEE Veh. Tech. Conf. (VTC)*. Performance of advanced receiver employing interference rejection combining to suppress inter-cell interference in LTE-Advanced downlink (San Francisco, 2011). doi:10.1109/VTECF.2011.6093196
 67. Renesas Mobile Europe Ltd.: 3GPP R1-111562 Interference aware receiver modeling at system level. Technical report (May 2011). [Online, last accessed 2015-01-26] <http://www.3gpp.org>
 68. M Sternad, S Falahati, T Svensson, D Aronsson, in *Proc. 14th European Information Society Technologies (IST) Mobile and Wireless Communications Summit*. Adaptive TDMA/OFDMA for wide-area coverage and vehicular velocities (Dresden, 2005)
 69. T Svensson, ChalmersUniversityofTechnology Dept. of Signals and System Goteborg, S Falahati, M Sternad, in *Paper presented at the IEEE 63rd vehicular technology conference*. Coding and resource scheduling in packet oriented adaptive TDMA/OFDMA systems (IEEE Melbourne, Vic., May 2006), p. 7–10
 70. 3GPP TR 36.872, Small cell enhancements for E-UTRA and E-UTRAN - physical layer aspects. Technical report (2013). [Online, last accessed 2014-10-01] <http://www.3gpp.org>
 71. V Chandrasekhar, JG Andrews, A Gatherer, Femtocell networks: a survey. *IEEE Commun. Mag.* **46**, 59–67 (2008). doi:10.1109/MCOM.2008.4623708
 72. LB Le, E Hossain, D Niyato, DI Kim, in *Proc. IEEE Int. Conf. on Commun. (ICC)*. Mobility-aware admission control with QoS guarantees in OFDMA femtocell networks, (2013). doi:10.1109/ICC.2013.6654857
 73. J Hare, L Hartung, S Banerjee, in *Proc. Int. Conf. on Mobile Systems, Applications, and Services (MobiSys)*. Beyond deployments and testbeds: experiences with public usage on vehicular WiFi hotspots (Low Wood Bay, 2012). doi:10.1145/2307636.2307673
 74. DJ Leith, P Clifford, in *Proc. Int. Symposium on Modeling and Optimization in Mobile, Ad Hoc, and Wireless Networks (WiOpt)*. A self-managed distributed channel selection algorithm for WLANs (Boston, 2006). doi:10.1109/WIOPT.2006.1666484
 75. VP Mhatre, K Papagiannaki, F Baccelli, in *IEEE Conf. on Computer Commun. (INFOCOM)*. Interference mitigation through power control in high density 802.11 WLANs (Anchorage, 2007)
 76. V Nurmela, A Karttunen, A Roivainen, L Raschkowski, T Imai, J Järveläinen, J Medbo, J Vihriälä, J Meinilä, J Kyröläinen, K Haneda, V Hovinen, J Ylitalo, N Omaki, V-M Kolmonen, K Kusume, P Kyösti, T Jämsä, ICT-317669-METIS/D1.2 Initial channel models based on measurements. Technical report (2014). [Online, last accessed 2014-10-01] <https://www.metis2020.com>
 77. J Medbo, K Börner, K Haneda, V Hovinen, T Imai, J Järveläinen, T Jämsä, A Karttunen, K Kusume, J Kyröläinen, P Kyösti, J Meinilä, V Nurmela, L Raschkowski, A Roivainen, J Ylitalo, in *Proc. European Conf. on Networks and Commun. (EuCNC)*. Channel modelling for the fifth generation mobile communications (Bologna, 2014)
 78. A Chen, in *Location- and Context-Awareness*, ed. by T Strang, C Linnhoff-Popien. Context-aware collaborative filtering system: predicting the user's preference in the ubiquitous computing environment (Springer Berlin, Germany, 2005), pp. 244–253

79. S Barmounakis, A Kalokylos, P Spapis, N Alonistioti, in *Proc. Int. Conf. on Advanced Commun. and Computation (INFOCOMP)*. CCompAsS: A context-aware, user-oriented RAT selection mechanism in heterogeneous wireless networks (Paris, 2014)
80. P Lungaro, Z Segall, J Zander, in *Proc. IEEE Wireless Commun. and Netw. Conf. (WCNC)*. ContextShift: a model for efficient delivery of content in mobile networks (Sydney, 2010)

Submit your manuscript to a SpringerOpen[®] journal and benefit from:

- ▶ Convenient online submission
- ▶ Rigorous peer review
- ▶ Immediate publication on acceptance
- ▶ Open access: articles freely available online
- ▶ High visibility within the field
- ▶ Retaining the copyright to your article

Submit your next manuscript at ▶ springeropen.com
